Abstract

Acknowledgments

Contents

G Simulation Design   **53**

Nomenclature

Chapter 1

Introduction

1.1 Context

In many applications of mechanical systems physical interaction with the environment is necessary to function, particularly in robotics. Humanoid robots, industrial robots, surgical robots are some examples of robotics that require physical interaction with their environment to function. Straight-forward control strategies that are available for these applications, are limiting in performance. To avoid complexity of the controller, they often assume contact with their environment to happen at zero speed. This makes the robots less suitable for situations where speed is of significance, e.g., for industrial or walking robots. Higher performance is desirable in such cases. However, making contact with your environment at non-zero velocities complicates the control problem.
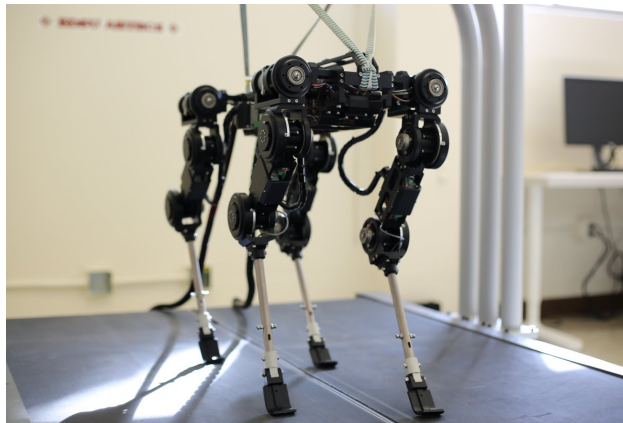
Figure 1.1: *The quadruped of Virginia Tech is an example of a robot with physical interaction that can benefit from high performance control strategies.*

When two bodies make physical contact at a considerable velocity, impact occurs. Impact is a complex physical event, that is characterized by very short durations, high force levels, high energy dissipation rates, and large accelerations and decelerations. Due to the small time scale at which impacts happen, the impact is often modeled by assuming that the change in velocity during impact happens due to an impulsive force, i.e., the velocity jump happens in zero time. Systems exhibiting such dynamics are often represented as *non-smooth*. In dynamics, the state doesn't necessarily have to be a smooth function of time, meaning that not all it's time-derivatives exist. Non-smooth mechanical systems with impact are systems that have discontinuities in their state-evolution. Me-

chanical systems with unilateral constraints are an example of systems that can exhibit non-smooth behavior, as they can jump in state when the unilateral constraints are closed. Control strategies for such systems are necessary to achieve better performance.

1.2 Non-smooth modeling frameworks

Non-smooth systems can be described by several mathematical frameworks, e.g., singularly perturbed systems, hybrid systems, complementarity systems and (measure-)differential inclusions [1]. The singular perturbation framework approximates the non-smooth behaviour using a singularly perturbed smooth system. In this way, the singularly perturbed system can be evaluated numerically using a single smooth differential equation. However, due to the smooth approximation extremely small time-steps are necessary which makes the system less suitable for simulation. More suitable for this are differential inclusions, which are applicable to systems with a discontinuous right-hand side but a time-continuous state-evolution (also called Filippov-systems) [2]. A common example of Filippov-systems are systems including friction. The differential inclusion gives a description of the non-smooth dynamics in a single inclusion. However, mechanical systems with unilateral constraints and impact do not satisfy the requirement of having a time-continuous state-evolution. A measure-differential inclusion describes the continuous as well as the impulsive dynamics of a non-smooth system [3]. In this way, measure-differential inclusions are suitable for systems with time-discontinuities in their state-evolution [4, 5]. Using this approach the dynamics can be accurately integrated using the timestepping method [6]. From a control point-of-view the complementarity framework is often considered. This framework describes non-smoothness through a combination of differential equations and inequalities [7, 8]. In [9] the complementarity problem is used to describe mechanical systems with unilateral constraints. It plays a key role in mathematical programming, and several solutions for trajectory tracking using complementarity systems exist [10, 11]. In recent years the hybrid systems framework has drawn more interest for solving the trajectory tracking problem of non-smooth systems [12, 13]. A hybrid system is a dynamical system that exhibits both continuous and discrete dynamics behaviour, where it switches (discrete behaviour) between several differential equations (continuous behaviour) [14]. *Guard functions* are defined, which when activated will cause the dynamics to switch from one differential equation to another and possibly reinitialize the state. This makes it a very intuitive approach to the modeling of non-smoothness. A known difficulty with this description however, is a phenomenon called Zeno-behaviour. One speaks of Zeno-behaviour when an infinite amount of guard activations happen in a finite time. A classic example is the bouncing ball. The framework of measure-differential inclusions would be more suitable in such a situation, because the impulsive dynamics are implicit in the inclusion. An advantage of using the hybrid systems framework, is that it is a more intuitive description of the dynamics whereas measure-differential inclusions are more abstract. The stability analyses for these frameworks are well-developed, i.e., [14–16] for hybrid systems, [17–19] for measure differential inclusions, and [5, 20, 21] for linear complementarity problems.

1.3 Trajectory tracking control for non-smooth systems

Legged robotic systems account for a substantial part of the research done into the trajectory tracking control of mechanical systems with unilateral constraints. Many results in this area deal with the stability of periodic orbits of systems with impacts. In [22], a first big step has been made into modeling and controlling a one-legged hopping robot. In this research, the energy-loss during impact is modelled through damping and coupling effects are modeled as perturbations. In [23],

the hybrid framework is adopted to find stable walking gaits for biped robots. Using Poincaré maps in [24], the stability of periodic orbits with discontinuities of under-actuated systems are analyzed. [25] continues on this work, generating control laws using data of walking humans and in [26] the energy-efficiency of generated walking gaits has been the focus. The analysis of stable walking gaits is applied to the MIT Cheetah in [12], where a stability analysis and controller design is presented for the trot-running of a quadrupedal robot. In [27, 28], quasi-stability is introduced for systems with periodic trajectories in the so-called *Birkhoff billiard*. This notion of stability defines asymptotic stability for the periodic trajectory, except for the time-instants where impacts happen.

There has been made considerable progress in the field of walking robots and billiards, but it is easy to think of a an example where non-periodic trajectories are of interest. Under the assumption that the state trajectory jumps at the exact same time as the reference trajectory, the trajectory tracking problem for non-smooth systems had been solved multiple times. The tracking problem for Lur'e type systems has been analyzed in [29, 30], using MDI's to describe non-smooth and impulsive dynamics. This work uses the convergence property to provide a solution to the tracking problem, where the solution may be time-varying and exhibit state-jumps. In [10], the passivity-based approach is used to solve the tracking control problem of complementarity Lagrangian systems. Asymptotic stability is achieved for Lagrangian systems with unilateral constraints. The same approach has been applied to the hybrid system framework in [31], which results in a control law that can guarantee stability of a trajectory with multiple impacts. By embedding the reference trajectory with discontinuities into a set, Lyapunov tools can be used to analyze stability as in [32, 33]. In [34] a stability analysis of systems with impacts and friction has been presented. The results are obtained using the measure-differential inclusion framework, resulting in a smooth control law.

In the prior discussed work, the tracking problem has often been solved under the assumption that the jump of the state occurs at the same time-instant as the jump of the desired trajectory, i.e., in [31, 33, 34]. In reality, especially in high velocity conditions, the state jump and trajectory jump do not always coincide. In this case a phenomenon called *peaking* occurs [35]. Spikes in the tracking error will arise around the jump times, which defy the notion of stability and are unfavorable when designing a stabilizing controller. Several solutions exist to solve this problem. Solutions exist for periodic orbits in [27, 28], where the results are compatible with a mismatch in reference jump-time and state jump-time. In [35, 36], a novel definition of the tracking error is introduced, using a distance function which is not sensitive to jumps of the state and the reference trajectory. Lyapunov-based conditions for the global asymptotic stability of non-smooth trajectories have been derived. Another solution for the problem of a jump-time mismatch is proposed in [37], in the form of a distance function similar to [35, 36] based on a quotient metric. When a state jump happens at different time than the reference jump, this approach applies the jump map to the reference to be able to compare the state to the reference. [38] introduces a novel controller design using gluing functions to connect the start and end point of a jump in the state space. After gluing, the system can be considered a continuous or piecewise continuous function without state jumps. In [39] a tracking error is defined by taking the smallest of two values: the ante-impact tracking error and post-impact tracking error.

1.4 Reference spreading control

In [40] a novel notion of error is defined by extending the reference trajectory segments over the entire domain of the state space, and considering the error between the trajectory and state that have encountered the same number of jumps. This notion of error, called *reference spreading*, is the basis for extending the sensitivity analysis introduced in [41] to the hybrid system framework.

These results are then used to obtain a local approximation of the perturbed state dynamics. This analysis gives insight in how the system behaves under the presence of perturbations, which is useful during controller design. In [42, 43], the sensitivity analysis for hybrid systems with state triggered jumps is used for a trajectory tracking control strategy, which is named *reference spreading control*. In [44] the reference spreading control law is used in simulations with an iCub robot. The iCub robot balances on one foot and keeps himself standing upright by making and breaking contact with a wall using on of his arms. Some snapshots of the motion are depicted in Figure 1.1. As mentioned earlier, many available results work under the assumption that the exact impact time is known. This is extremely limiting during implementation of the control law. Using the reference spreading approach, the impact time of the state is allowed to deviate from that of the reference, making implementation of the control law in practical applications more viable while still allowing for state-jumps.
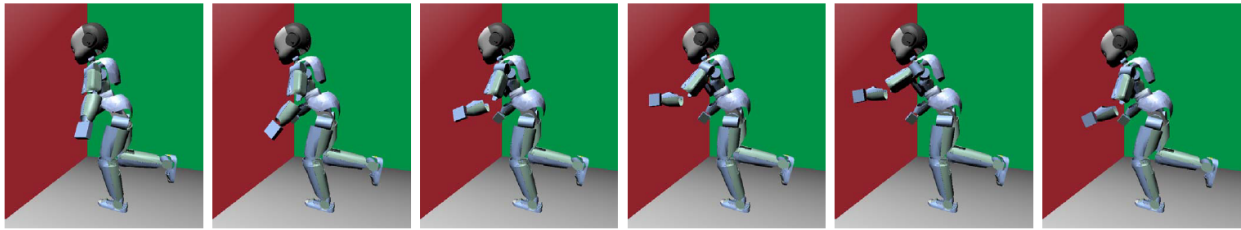

Figure 1.1: *Snapshots of the motion the iCub robot makes in the simulation done in [44] using reference spreading control.*

Talk about simulation Mark, and then from ordered to simultaneous Impacts are often modeled using one point contact between two bodies. However, in practice more complex geometries can make contact with each other. A more realistic contact is used in [45], in which a humanoid bipedal robot is modeled with multiple impacts when one of it's feet makes contact with the ground. One contact is modeled by a heel impact, a toe impact, a heel release, and finally a toe release; a series of impacts that happen in a certain order.

When such geometries make contact, one can imagine that the order of impacts is not always known. Imagine for example the iCub in [44] having a physically realistic geometry at the end of it's arm. The arm can first make a point contact, then a line contact, and finally a surface contact in rapid succession. However, at high velocities, these impacts will happen at an instant, and small perturbations can change the order of impact. When several impacts happen at the same time-instant, they can be called *simultaneous impacts*. The approach used in [45] is not suitable for these challenging situations.

The phenomenon of simultaneous impacts is first introduced in [46], where the first step is taken into solving the trajectory tracking problem for such impacts. A hybrid system framework is used to model the impacts, where multiple guards can be activated at once. The reference spreading control in [42,43] and the sensitivity analysis to approximate a system's behavior around trajectories with single guard activation, introduced in [40], are extended to be suitable for simultaneous guard activation. The results of the sensitivity analyses are used to find suitable gains for the reference spreading control law. However, these results do not consider friction. In addition to an impulse perpendicular to the impact-surface, taking friction into account will result in a tangential impulse. Also the release phase is not considered in the work of [46]. During the release phase there is no discontinuity in the state-evolution, only a change in the number of active constraints on the system. Therefore, the aim of this research is to investigate both stability of impacts including friction and the release phase of contact.

1.5   Contribution

Simultaneous impacts with friction

Friction elements are often disregarded when analyzing impacts. However, to set up a unifying theory friction elements should not be ignored. Tangential impulses can have a considerable effect on a system's dynamics. The impact laws used in the work of [46] can be extended using one of the several available friction laws [19]. When impact laws are supplemented with a tangential element, this is often done using a Coulomb friction law [47]. Besides the tangential impulse, also a Filippov-like discontinuity will be present due to Coulomb friction. Also in this work a Coulomb friction law is used, which can lead to more accurate models and controllers for mechanical systems with unilateral constraints.

Research Objective:
Find a model suitable to describe mechanical systems with unilateral constraints and spatial friction. The positive homogenization's notation and sensitivity analysis shall be adjusted to be compatible with such models.

Simultaneous impacts with release

In [42] and [48], the release phase of a system with a reference spreading controller has been extensively researched. However, these results only include single guard activation. The release phase for multiple guard activation is not yet investigated. In [46], only a single contact is simulated for this reason. Extending the sensitivity analysis in [46] to be suitable for simultaneous releases would make it possible to simulate and control one trajectory with several simultaneous contacts and releases.

Research Objective:
Adjusting the positive homogenization, such that it is suitable for input-dependent guard functions. This will result in a positive homogenization suitable for trajectories that contain a releasing motion.

1.6   Report Outline

Chapter 2

Modeling of Mechanical Systems with Unilateral Constraints and Spatial Friction

2.1 Nonlinear complementarity problems

2.2 Hybrid systems

Chapter 3

Trajectory Tracking Control for Hybrid Systems with State-Triggered Jumps

[43]

Chapter 4

The Positive Homogenization

[49]

4.1 Adopted Notation

4.2 Positive Homogenization for Trajectories with Simultaneous Guard-Activation

Chapter 5

Numerical Validation

Chapter 6

Conclusions and Recommendations

Bibliography

[1] Remco I. Leine and Henk Nijmeijer. *Dynamics and Bifurcations of Non-Smooth Mechanical Systems*. Springer-Verlag, Berlin, Heidelberg, 1st edition, 2004.

[2] A. F. Filippov. *Differential Equations with Discontinuous Righthand Sides*. Springer-Science, Dordrecht, 1st edition, 1988.

[3] Remco I. Leine and Nathan Van De Wouw. Uniform Convergence of Monotone Measure Differential Inclusions: With Application To the Control of Mechanical Systems With Unilateral Constraints. *International Journal of Bifurcation and Chaos*, 18(5):1435–1457, 2008.

[4] J. J. Moreau and P. O. Panagiotopoulos. *Nonsmooth Mechanics and Applications*. Springer-Verlag, Wien, 1st edition, 1988.

[5] Bernard Brogliato. *Nonsmooth Mechanics*. Springer, 3rd edition, 1999.

[6] N Van De Wouw. An introduction to Time-Stepping: a Numerical Technique for Mechanical Systems with Unilateral Constraints. pages 1–27.

[7] A. J. Van Der Schaft and J. M. Schumacher. Complementarity modeling of hybrid systems. *IEEE Transactions on Automatic Control*, 43(4):483–490, 1998.

[8] W. Heemels. Linear complementarity systems: a study in hybrid dynamics. (november):1–241, 1999.

[9] Christoph Glocker. *Set-Valued Force Laws: Dynamics of Non-Smooth SystemsÂ (Google eBook)*, volume 1. 2001.

[10] Jean-Matthieu Bourgeot and Bernard Brogliato. Passivity-based tracking control of multiconstraint complementarity Lagrangian systems. *International Journal of Bifurcation and Chaos*, 15(6):1839–1866, 2005.

[11] Irinel-Constantin Morarescu and Bernard Brogliato. Tracking Control of Multiconstraint Complementarity Lagrangian Systems. *International Journal of Bifurcation and Chaos*, 55(6):1300–1313, 2010.

[12] Dong Jin Hyun, Sangok Seok, Jongwoo Lee, and Sangbae Kim. High speed trot-running: Implementation of a hierarchical controller using proprioceptive impedance control on the MIT Cheetah. *International Journal of Robotics Research*, 33(11):1417–1445, 2014.

[13] Benjamin Morris and Jessy W. Grizzle. Hybrid invariant manifolds in systems with impulse effects with application to periodic locomotion in bipedal robots. *IEEE Transactions on Automatic Control*, 54(8):1751–1764, 2009.

[14] Rafal Goebel, Ricardo G. Sanfelice, and Andrew R. Teel. Hybrid dynamical systems. *IEEE Control Systems Magazine*, 29(2):28–93, 2009.

[15] Hui Ye and a. N. Michel. Stability theory for hybrid dynamical systems. *IEEE Transactions on Automatic Control*, 43(4):461–474, 1998.

[16] J. Lygeros, K.H. Johansson, S.N. Simic, and S.S. Sastry. Dynamical properties of hybrid automata. *IEEE Transactions on Automatic Control*, 48(1):2–17, 2003.

[17] F. L. Pereira and G. N. Silva. Lyapunov stability of measure driven impulsive systems. *Differential Equations*, 40(8):1122–1130, 2004.

[18] Bernard Brogliato. Absolute stability and the Lagrange-Dirichlet theorem with monotone multivalued mappings. *Systems and Control Letters*, 51(5):343–353, 2004.

[19] R.I. Leine and N. van de Wouw. *Stability and Convergence of Mechanical Systems with Unilateral Constraints*, volume 36. Springer, 2008.

[20] M Kanat Camlibel, Jong-Shi Pang, and Jinglai Shen. Lyapunov Stability of Complementarity and Extended Systems. *SIAM Journal on Optimization*, 17(4):1056–1101, 2007.

[21] M. Kanat Camlibel and Nathan Van De Wouw. On the Convergence of Linear Passive Complementarity Systems. *IEEE Conference on Decision and Control*, 46th:5886–5891, 2007.

[22] Marc H. Raibert. Hopping in Legged Systems - Modeling and Simulation for the Two-Dimensional One-Legged Case. *IEEE Transactions on Systems, Man and Cybernetics*, SMC-14(3):451–463, 1984.

[23] Jesse W. Grizzle, Gabriel Abba, and Franck Plestan. Asymptotically stable walking for biped robots: Analysis via systems with impulse effects. *IEEE Transactions on Automatic Control*, 46(1):51–64, 2001.

[24] T. S. Parker and L.O. Chua. *Practical numerical algorithms for chaotic systems*. Springer-Verlag, New York, 1st edition, 1989.

[25] Aaron D. Ames. Human-inspired control of Bipedal walking robots. *IEEE Transactions on Automatic Control*, 59(5):1115–1130, 2014.

[26] Jacob Reher, Eric A. Cousineau, Ayonga Hereid, Christian M. Hubicki, and Aaron D. Ames. Realizing dynamic and efficient bipedal locomotion on the humanoid robot DURUS. *Proceedings - IEEE International Conference on Robotics and Automation*, 2016-June:1794–1801, 2016.

[27] Laura Menini and Antonia Tornambè. Asymptotic tracking of periodic trajectories for a simple mechanical system subject to nonsmooth impacts. *IEEE Transactions on Automatic Control*, 46(7):1122–1126, 2001.

[28] S. Galeani, L. Menini, A. Potini, and A. Tornambè. Trajectory tracking for a particle in elliptical billiards. *International Journal of Control*, 81(2):189–213, 2008.

[29] Nathan van de Wouw and Remco I Leine. Tracking control for a class of measure differential inclusions. *Proceedings IEEE Conference on Decision and Control*, pages 2526–2532, 2008.

[30] Nathan Van De Wouw and Remco I Leine. Stability and Control of Lur'e-type Measure Differential Inclusions. pages 129–151, 2010.

[31] Roberto Naldi and Ricardo G. Sanfelice. Passivity-based control for hybrid systems with applications to mechanical systems exhibiting impacts. *Automatica*, 49(5):1104–1116, 2013.

[32] Ricardo G. Sanfelice, J. J. Benjamin Biemond, Nathan Van De Wouw, and W. P. Maurice H. Heemels. Tracking control for hybrid systems via embedding of known reference trajectories. *Proceedings of the 2011 American Control Conference*, (4):869–874, 2011.

[33] Ricardo G. Sanfelice, J. J.Benjamin Biemond, Nathan Van De Wouw, and W. P. Maurice H. Heemels. An embedding approach for the design of state-feedback tracking controllers for references with jumps. *International Journal of Robust and Nonlinear Control*, 24:1585–1608, 2014.

[34] Michael Posa, Mark Tobenkin, and Russ Tedrake. Stability Analysis and Control of Rigid Body Systems with Impacts and Friction. *IEEE TRANSACTIONS ON AUTOMATIC CONTROL*, 61(6):1423–1437, 2016.

[35] J J B Biemond, N Van De Wouw, W P M H Heemels, and H Nijmeijer. Tracking Control for Hybrid Systems with State-Triggered Jumps. *IEEE Transactions on Automatic Control*, 58(257462):876–890, 2013.

[36] J. J.Benjamin Biemond, W. P.Maurice H. Heemels, Ricardo G. Sanfelice, and Nathan van de Wouw. Distance function design and Lyapunov techniques for the stability of hybrid trajectories. *Automatica*, 73:38–46, 2016.

[37] Michael Baumann, J. J.Benjamin Biemond, Remco I. Leine, and Nathan van de Wouw. Synchronization of impacting mechanical systems with a single constraint. *Physica D: Nonlinear Phenomena*, 362:9–23, 2018.

[38] Jisu Kim, Hyungbo Shim, and Jin Heon Seo. Tracking control for hybrid systems with state jumps using gluing function. *2016 IEEE 55th Conference on Decision and Control, CDC 2016*, (Cdc):3006–3011, 2016.

[39] Ting Yang, Fen Wu, and Lixian Zhang. Tracking control of hybrid systems with state-triggered jumps and stochastic events and its application. *IET Control Theory & Applications*, 11(7):1024–1033, 2017.

[40] Alessandro Saccon, Nathan van de Wouw, and Henk Nijmeijer. Sensitivity analysis of hybrid systems with state jumps with application to trajectory tracking. *Proceedings of the 53rd IEEE Conference on Decision and Control*, pages 3065–3070, 2014.

[41] Hassan K. Khalil. *Nonlinear Systems*. Number 3rd. Prentice-Hall, Englewood Cliffs, NJ, 1996.

[42] M. W.L.M. Rijnen, A. T. van Rijn, H. Dallali, A. Saccon, and H. Nijmeijer. Hybrid Trajectory Tracking for a Hopping Robotic Leg. *IFAC-PapersOnLine*, 49(14):107–112, 2016.

[43] M. W.L.M. Rijnen, J. J.Benjamin Biemond, Alessandro Saccon, Nathan Van De Wouw, and Henk Nijmeijer. Hybrid Systems with State-Triggered Jumps: Sensitivity-Based Stability Analysis with Application to Trajectory Tracking. pages 1–16, 2017.

[44] Mark Rijnen, Eric De Mooij, Silvio Traversaro, Francesco Nori, Nathan Van De Wouw, Alessandro Saccon, and Henk Nijmeijer. Control of humanoid robot motions with impacts: Numerical experiments with reference spreading control. *Proceedings - IEEE International Conference on Robotics and Automation*, pages 4102–4107, 2017.

[45] Huihua Zhao, Jonathan Horn, Jacob Reher, Victor Paredes, and Aaron D. Ames. A hybrid systems and optimization-based control approach to realizing multi-contact locomotion on transfemoral prostheses. *Proceedings of the IEEE Conference on Decision and Control*, 54(2):1607–1612, 2015.

[46] Hao Liang Chen. *Trajectory tracking control for mechanical systems experiencing simultaneous impacts*. Master's thesis, Eindhoven University of Technology, 2018.

[47] Christoph Glocker. Energetic consistency conditions for standard impacts: Part I: Newton-type inequality impact laws and Kane's example. *Multibody System Dynamics*, 32(4):445–509, 2014.

[48] Anthom van Rijn. *Hybrid trajectory tracking for hopping robots*. Master's thesis, Eindhoven University of Technology, 2016.

[49] Mark Rijnen, Hao Liang Chen, Nathan Van De Wouw, Alessandro Saccon, and Henk Nijmeijer. Sensitivity analysis for trajectories of nonsmooth mechanical systems with simultaneous impacts : a hybrid systems perspective. 2018.

Appendix A

Mathematical Preliminaries

Appendix B

Modeling of Mechanical Systems with Unilateral Constraints with Spatial Friction

B.1   Complementarity condition formulation

Flow Dynamics

$\mathcal{I}_a$ is the set of all possible contacts, $\mathcal{I}_c$ the set of closed contacts, $\mathcal{I}_{sl}$ the set of contacts in slip, and $\mathcal{I}_{st}$ the set of contacts in stick with $\mathcal{I}_c \subseteq \mathcal{I}_a$, $\mathcal{I}_c = \mathcal{I}_{sl} \cup \mathcal{I}_{st}$ and $\mathcal{I}_{sl} \cap \mathcal{I}_{st} = \emptyset$. When considering the expression $x \perp y$, he symbol $\perp$ is used to express the orthogonality between x and y. We define $\boldsymbol{\xi} = \dot{\boldsymbol{q}}$, except at jump-times τ_i. h_n is the normal contact distance and ζ_n and ζ_t represent the relative velocities in normal and tangential direction, respectively. The function $\epsilon(x)$ is defined as

$$\epsilon(x) = \left\{ \begin{array}{cl} \frac{x}{||x||}, & \text{if } x \neq 0 \\ 0, & \text{if } x = 0 \end{array} \right. . \tag{B.1}$$

Then

$$\boldsymbol{M}(\boldsymbol{q})\dot{\boldsymbol{\xi}} + \boldsymbol{H}(\boldsymbol{q}, \boldsymbol{\xi}) = \boldsymbol{S}(\boldsymbol{q})\boldsymbol{u} + \sum_{i \in \mathcal{I}_c} \left(\boldsymbol{w}_{n,i}(\boldsymbol{q})\lambda_{n,i} + \boldsymbol{W}_{t,i}(\boldsymbol{q})\boldsymbol{\lambda}_{t,i} \right), \tag{B.2}$$

$$0 \leq h_{n,i} \perp \lambda_{n,i} \geq 0, \qquad \forall i \in \mathcal{I}_a \tag{B.3}$$

$$0 \leq \mu\lambda_{n,i} - ||\boldsymbol{\lambda}_{t,i}|| \perp \kappa_i \geq 0, \qquad \forall i \in \mathcal{I}_c \tag{B.4}$$

$$\boldsymbol{\zeta}_{t,i} = \kappa_i \boldsymbol{\lambda}_{t,i} \qquad \forall i \in \mathcal{I}_c, \tag{B.5}$$

with

$$\zeta_{n,i}(\boldsymbol{q}) = \boldsymbol{w}_{n,i}^T(\boldsymbol{q})\boldsymbol{\xi}, \tag{B.6}$$

$$\boldsymbol{\zeta}_{t,i}(\boldsymbol{q}) = \boldsymbol{W}_{t,i}^T(\boldsymbol{q})\boldsymbol{\xi}. \tag{B.7}$$

Impact Dynamics

$$M(\boldsymbol{q})(\boldsymbol{\xi}^+ - \boldsymbol{\xi}^-) = \sum_{i \in \mathcal{I}_c} \left(\boldsymbol{w}_{n,i}(\boldsymbol{q})\Lambda_{n,i} + \boldsymbol{W}_{t,i}(\boldsymbol{q})\boldsymbol{\Lambda}_{t,i} \right), \tag{B.8}$$

$$0 \leq \zeta_{n,i}^+ \perp \Lambda_{n,i} \geq 0, \qquad \forall i \in \mathcal{I}_c \tag{B.9}$$

$$0 \leq \mu\Lambda_{n,i} - ||\boldsymbol{\Lambda}_{t,i}|| \perp \kappa_i \geq 0. \qquad \forall i \in \mathcal{I}_c \tag{B.10}$$

$$\boldsymbol{\zeta}_{t,i}^+ = \kappa_i \boldsymbol{\Lambda}_{t,i} \qquad \forall i \in \mathcal{I}_c \tag{B.11}$$

with

$$\zeta_{n,i}^+(\boldsymbol{q}) = \boldsymbol{w}_{n,i}^T(\boldsymbol{q})\boldsymbol{\xi}^+, \tag{B.12}$$

$$\boldsymbol{\zeta}_{t,i}^+(\boldsymbol{q}) = \boldsymbol{W}_{t,i}^T(\boldsymbol{q})\boldsymbol{\xi}^+. \tag{B.13}$$

B.2 Proximal point formulation

B.2.1 Proximal point formulation of contact law

B.2.2 Proximal point formulation of friction law

In Figure B.1 a convex set C is illustrated. The normal cone $N_C(\boldsymbol{x})$ of a point $\boldsymbol{x}$ is $N_C(\boldsymbol{x}) = 0$ if $\boldsymbol{x} \in \text{int}(C)$, where int(.) is the interior of a set. An example of this is point $\boldsymbol{x}_3$ in Figure B.1. Defining bd(.) as the boundary of the set, when $\boldsymbol{x} \in \text{bd}(C)$ there are two options. When $\boldsymbol{x}$ is on a smooth part of bd(C), then $N_C(\boldsymbol{x})$ is a ray normal to bd(C) at point $\boldsymbol{x}$ as depicted in at point $\boldsymbol{x}_1$. When $\boldsymbol{x}$ is on a non-smooth part of bd(C), then $N_C(\boldsymbol{x})$ is a cone starting on the point $\boldsymbol{x}$ whose sides are normal to the left and right approximation of the point $\boldsymbol{x}$ on bd(C). This is illustrated at point $\boldsymbol{x}_2$. The proximal point $\text{prox}_C(\boldsymbol{z})$ of a point $\boldsymbol{z}$, is the point in C closest to the point $\boldsymbol{z}$. The point $\boldsymbol{x}$ is the proximal point to all points $\boldsymbol{z} \in N_C(\boldsymbol{x})$. For a point $\boldsymbol{z} \in C$, $\text{prox}_C(\boldsymbol{z}) = \boldsymbol{z}$ i.e. $\boldsymbol{x}_3$ in Figure B.1.

Now we define the normal cone formulation

$$-\dot{\boldsymbol{h}}_{t,i} \in N_{C_{t,i}}(\boldsymbol{\lambda}_{t,i}) \quad \forall i \in \mathcal{I}_a, \quad \text{with } C_{t,i} = \{\boldsymbol{\lambda}_{t,i} \mid ||\boldsymbol{\lambda}_{t,i}|| \leq \mu\lambda_{n,i}\}, \tag{B.14}$$

which is illustrated in Figure B.2. C_t is the set of all admitted friction forces. The tangential velocity $\dot{\boldsymbol{h}}_{t,i}$ is directed opposite to the friction force $\boldsymbol{\lambda}_{t,i}$ for isotropic friction.

Now using the fact that

$$\boldsymbol{x} = \text{prox}_C(\boldsymbol{x} - r\boldsymbol{y}), r > 0 \iff -\boldsymbol{y} \in N_C(\boldsymbol{x}), \tag{B.15}$$

we can rewrite the normal cone to a proximal point formulation

$$\boldsymbol{\lambda}_{t,i} = \text{prox}_{C_{t,i}}(\boldsymbol{\lambda}_{t,i} - r\dot{\boldsymbol{h}}_{t,i}) \quad \forall i \in \mathcal{I}_a \quad \text{with } C_{t,i} = \{\boldsymbol{\lambda}_{t,i} \mid ||\boldsymbol{\lambda}_{t,i}|| \leq \mu\lambda_{n,i}\} \text{ and } r > 0. \tag{B.16}$$

Similarly, for the impact dynamics we can formulate

$$\boldsymbol{\Lambda}_{t,i} = \text{prox}_{C_{t,i}}(\boldsymbol{\Lambda}_{t,i} - r\dot{\boldsymbol{h}}_{t,i}^+) \quad \forall i \in \mathcal{I}_a \quad \text{with } C_{t,i} = \{\boldsymbol{\Lambda}_{t,i} \mid ||\boldsymbol{\Lambda}_{t,i}|| \leq \mu\Lambda_{n,i}\} \text{ and } r > 0. \tag{B.17}$$
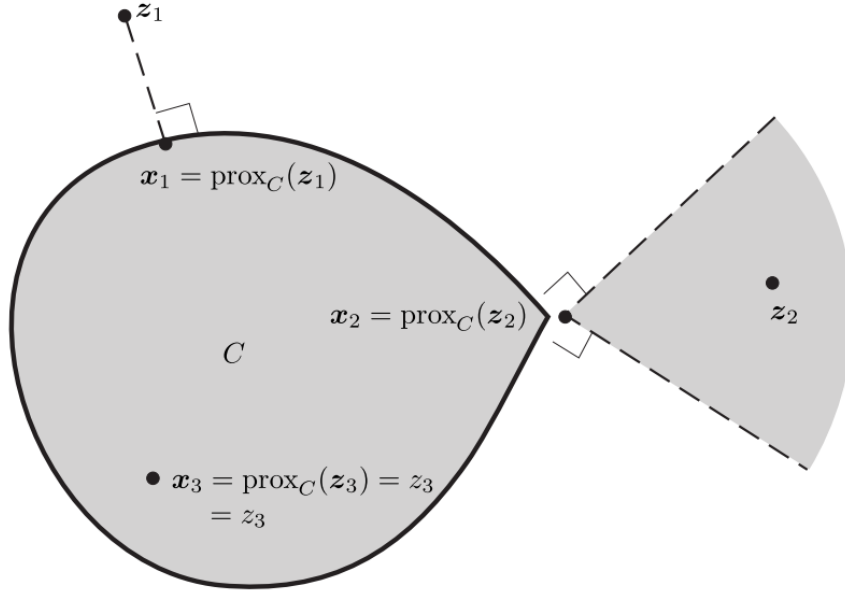
Figure B.1

B.3 Hybrid system formulation for mechanical system with unilateral constraints and spatial friction

In this section the dynamics of the complementarity system defined in the section above is written to a hybrid formulation. This formulation is less formal than the complementarity formulation, which is entirely mathematically correct. The hybrid formulation is used to give a more intuitive approach to simulating a system with impacts.

B.3.1 Jump map formulation

The impact dynamics related to the jump sets are given by

$$0 \leftarrow * :$$
$$(\dot{\boldsymbol{q}}^+ - \dot{\boldsymbol{q}}^-) = 0, \tag{B.18}$$
$$1 \leftarrow * :$$
$$\boldsymbol{M}(\boldsymbol{q})(\dot{\boldsymbol{q}}^+ - \dot{\boldsymbol{q}}^-) = \boldsymbol{w}_{n,i}(\boldsymbol{q})\Lambda_{n,i} + \boldsymbol{W}_{t,i}(\boldsymbol{q})\boldsymbol{\Lambda}_{t,i}, \tag{B.19}$$
$$\zeta_{n,i}^+ = 0, \tag{B.20}$$
$$\boldsymbol{\Lambda}_{t,i} = -\epsilon(\boldsymbol{\zeta}_{t,i}^-)\mu\Lambda_{n,i}, \tag{B.21}$$
$$2 \leftarrow * :$$
$$\boldsymbol{M}(\boldsymbol{q})(\dot{\boldsymbol{q}}^+ - \dot{\boldsymbol{q}}^-) = \boldsymbol{w}_{n,i}(\boldsymbol{q})\Lambda_{n,i} + \boldsymbol{W}_{t,i}(\boldsymbol{q})\boldsymbol{\Lambda}_{t,i}, \tag{B.22}$$
$$\zeta_{n,i}^+ = 0, \tag{B.23}$$
$$\zeta_{t,i}^+ = 0, \tag{B.24}$$

with $0 \leftarrow *, 1 \leftarrow *$ and $2 \leftarrow *$ representing the impact dynamics to open contact, slip and stick respectively and $\epsilon(x)$ as defined in (B.1).

Figure B.2: *The friction disk with two seperate friction forces $\boldsymbol{\lambda}_{t,1}$ and $\boldsymbol{\lambda}_{t,2}$. $\boldsymbol{\lambda}_{t,1} = \mu\lambda_{n,1}$, resulting in a tangenti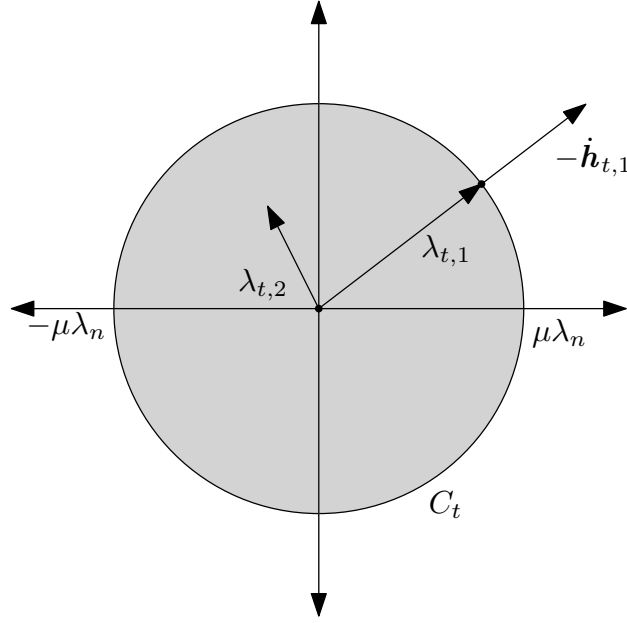al velocity $\dot{\boldsymbol{h}}_{t,i} > 0$. $\boldsymbol{\lambda}_{t,2} < \mu\lambda_{n,2}$, leading to a tangential velocity $\dot{\boldsymbol{h}}_{t,i} = 0$.*

When we go from any mode to open, there is no jump in the velocity and the reaction impulses are 0. Therefore $0 \leftarrow *$ is correct.

When we go from open to slip, there will be a jump in velocity, and $||\boldsymbol{\Lambda}_{t,i}|| = \mu\Lambda_{n,i}$. The reaction impulses will be larger than zero. When we go from stick to slip, there will be no jump in velocity. In stick, $\boldsymbol{\zeta}_{t,i} = 0$, so $\epsilon(\boldsymbol{\zeta}_{t,i}^-) = 0$. Also we know $\boldsymbol{w}_{n,i}^T\dot{\boldsymbol{q}}^- = \boldsymbol{w}_{n,i}^T\dot{\boldsymbol{q}}^+ = 0$. This leads to $\dot{\boldsymbol{q}}^- = \dot{\boldsymbol{q}}^+$, meaning there is no jump in velocity and no impulsive reaction force. Therefore $1 \leftarrow *$ is correct.

When we go from open to stick, there will be a jump in velocity and impulsive reaction forces. **NOT FINISHED, WE HAVE TO HAVE SOME KIND OF PROOF THESE JUMP MAPS ARE CORRECT**

B.3.2 Guard-function formulation

Open to stick/slip
When a contact point is "open", it can trigger a guard function γ to go from open to closed. The plane that spans $\gamma = 0$ is divided in two regions: a region where the post-impact state is in slip and a region where the post-impact state is in stick. This region is defined by Γ, where $\Gamma < 0$ in the region where the contact point goes to slip and $\Gamma > 0$ in the region where the contact point goes to stick. When $\Gamma = 0$ the system is right at the border between a slip post-impact state and a stick post-impact state. This is illustrated in Figure B.1.
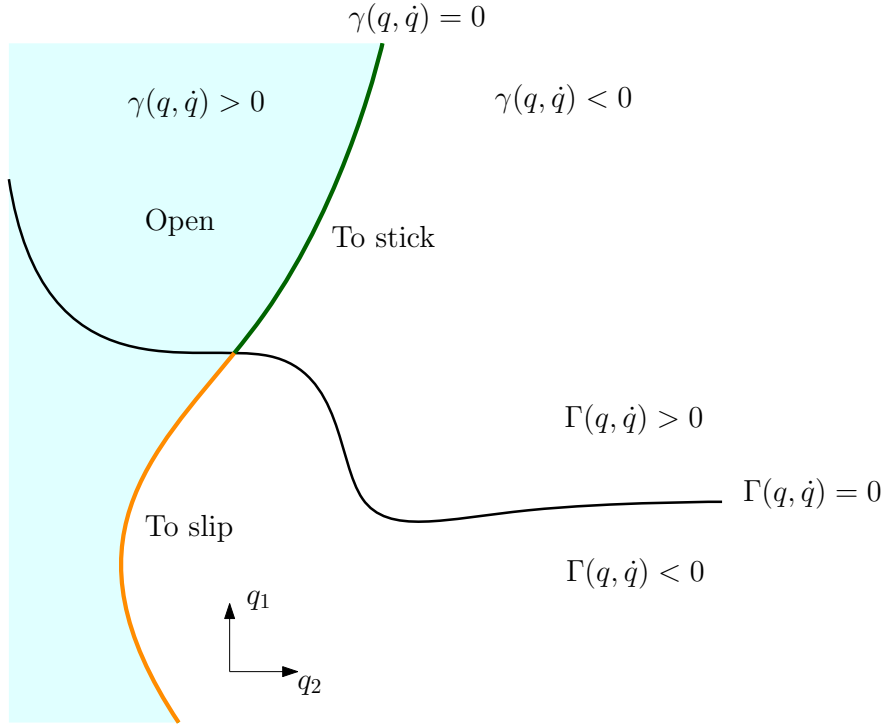
Figure B.1: *The functions* $\boldsymbol{\gamma}(\boldsymbol{q}, \dot{\boldsymbol{q}})$ *and* $\boldsymbol{\Gamma}(\boldsymbol{q}, \dot{\boldsymbol{q}})$ *illustrated in the state space of* $\boldsymbol{q} \in \mathbb{R}^2$. *The light blue area is the state space where the contact is open, and goes the closed when it triggers* $\gamma = 0$. *If it triggers* $\gamma = 0$ *in the area where* $\Gamma < 0$ *(orange), then the contact will go to slip. If it triggers* $\gamma = 0$ *in the area where* $\Gamma \geq 0$ *(green), then the contact will go to stick.*

For slip, we know that $\mu\Lambda_{n,i} - ||\boldsymbol{\Lambda}_{t,i}|| = 0$ and for stick, we know that $\mu\Lambda_{n,i} - ||\boldsymbol{\Lambda}_{t,i}|| \geq 0$. From this we can derive the guard function

$$\Gamma = \mu^2\Lambda_{n,i}^2(\boldsymbol{q}, \dot{\boldsymbol{q}}^-) - \boldsymbol{\Lambda}_{t,i}(\boldsymbol{q}, \dot{\boldsymbol{q}}^-)\boldsymbol{\Lambda}_{t,i}^T(\boldsymbol{q}, \dot{\boldsymbol{q}}^-). \tag{B.25}$$

This guard function Γ satisfies the requirements that $\Gamma < 0$ in the region where the contact point goes to slip, $\Gamma > 0$ in the region where the contact point goes to stick and $\Gamma = 0$ at the border. Even though it is not physically realistic that $\Gamma < 0$, it can still be used as a guard-function. We now find expressions for $\Lambda_{n,i}$ and $\boldsymbol{\Lambda}_{t,i}$ by looking at the jump map to stick, given in (B.22) to (B.24).

We can rewrite (B.22) to

$$\dot{\boldsymbol{q}}^+ = \boldsymbol{M}^{-1}\boldsymbol{w}_{n,i}\Lambda_{n,i} + \boldsymbol{M}^{-1}\boldsymbol{W}_{t,i}\boldsymbol{\Lambda}_{t,i} + \dot{\boldsymbol{q}}^-, \tag{B.26}$$

which after substituting into (B.23) and (B.24) lead to

$$\boldsymbol{w}_{n,i}^T\boldsymbol{M}^{-1}\boldsymbol{w}_{n,i}\Lambda_{n,i} + \boldsymbol{w}_{n,i}^T\boldsymbol{M}^{-1}\boldsymbol{W}_{t,i}\boldsymbol{\Lambda}_{t,i} + \zeta_{n,i}^- = 0 \tag{B.27}$$

$$\boldsymbol{W}_{t,i}^T\boldsymbol{M}^{-1}\boldsymbol{w}_{n,i}\Lambda_{n,i} + \boldsymbol{W}_{t,i}^T\boldsymbol{M}^{-1}\boldsymbol{W}_{t,i}\boldsymbol{\Lambda}_{t,i} + \boldsymbol{\zeta}_{t,i}^- = 0, \tag{B.28}$$

respectively, with $\zeta_{n,i}^- = \boldsymbol{w}_{n,i}^T\dot{\boldsymbol{q}}^-$ and $\boldsymbol{\zeta}_{t,i}^- = \boldsymbol{W}_{t,i}^T\dot{\boldsymbol{q}}^-$. This is now rewritten to

$$\begin{bmatrix} \boldsymbol{w}_{n,i}^T\boldsymbol{M}^{-1}\boldsymbol{w}_{n,i} & \boldsymbol{w}_{n,i}^T\boldsymbol{M}^{-1}\boldsymbol{W}_{t,i} \\ \boldsymbol{W}_{t,i}^T\boldsymbol{M}^{-1}\boldsymbol{w}_{n,i} & \boldsymbol{W}_{t,i}^T\boldsymbol{M}^{-1}\boldsymbol{W}_{t,i} \end{bmatrix} \begin{bmatrix} \Lambda_{n,i} \\ \boldsymbol{\Lambda}_{t,i} \end{bmatrix} + \begin{bmatrix} \zeta_{n,i}^- \\ \boldsymbol{\zeta}_{t,i}^- \end{bmatrix} = 0, \tag{B.29}$$

which is in turn rewritten to

$$\begin{bmatrix} \Lambda_{n,i} \\ \boldsymbol{\Lambda}_{t,i} \end{bmatrix} = -\boldsymbol{D}^{-1} \begin{bmatrix} \zeta_{n,i}^- \\ \boldsymbol{\zeta}_{t,i}^- \end{bmatrix}, \quad \text{with } \boldsymbol{D} = \begin{bmatrix} \boldsymbol{w}_{n,i}^T \boldsymbol{M}^{-1} \boldsymbol{w}_{n,i} & \boldsymbol{w}_{n,i}^T \boldsymbol{M}^{-1} \boldsymbol{W}_{t,i} \\ \boldsymbol{W}_{t,i}^T \boldsymbol{M}^{-1} \boldsymbol{w}_{n,i} & \boldsymbol{W}_{t,i}^T \boldsymbol{M}^{-1} \boldsymbol{W}_{t,i} \end{bmatrix}. \tag{B.30}$$

The matrix $\boldsymbol{D}$ is often called the Delassus-matrix. We now have expressions for $\Lambda_{n,i}$ and $\boldsymbol{\Lambda}_{t,i}$ which are continuous and differentiable in $(\boldsymbol{q}, \dot{\boldsymbol{q}})$. It is straightforward that $\Gamma(\boldsymbol{q}, \dot{\boldsymbol{q}})$ is continuous and differentiable as well. From the continuity of $\boldsymbol{\Gamma}_i$ we can say that if we trigger γ away from $\boldsymbol{\Gamma}_i = 0$, an infinitesimally small perturbation can not cause us to trigger γ on the other side of $\boldsymbol{\Gamma}_i$. This is proven in **SECTION TO BE WRITTEN**
Stick/slip to open

Stick to slip and slip to stick

B.3.3   Hybrid system formulation

$$\boldsymbol{M}(\boldsymbol{q})\ddot{\boldsymbol{q}} + \boldsymbol{H}(\boldsymbol{q}, \dot{\boldsymbol{q}}) = \boldsymbol{S}(\boldsymbol{q})\boldsymbol{u} + \sum_{i \in \mathcal{I}_c} \left(\boldsymbol{w}_{n,i}(\boldsymbol{q})\lambda_{n,i} + \boldsymbol{W}_{t,i}(\boldsymbol{q})\boldsymbol{\lambda}_{t,i} \right), \tag{B.31}$$

where every contact point in the set $\mathcal{I}_a$ is subjected to some set of constraints c_i, depending on the mode the contact point is in. These constraints are defined below:
Open (0):

$$c_{0,i}:$$
$$\lambda_{n,i} = 0 \tag{B.32}$$
$$\boldsymbol{\lambda}_{t,i} = 0 \tag{B.33}$$

with the jump sets

$$^{1\leftarrow 0}\mathcal{D} = \{\boldsymbol{q}, \boldsymbol{u} \in \mathbb{R}^n \mid h_{n,i} = 0, \ \Lambda_{n,i}^2 - \boldsymbol{\Lambda}_{t,i}\boldsymbol{\Lambda}_{t,i}^T = 0\}, \tag{B.34}$$
$$^{2\leftarrow 0}\mathcal{D} = \{\boldsymbol{q}, \boldsymbol{u} \in \mathbb{R}^n \mid h_{n,i} = 0, \ \Lambda_{n,i}^2 - \boldsymbol{\Lambda}_{t,i}\boldsymbol{\Lambda}_{t,i}^T > 0\}. \tag{B.35}$$

The derivation of these jump sets is given in Section B.3.1.
Slip (1):

$$c_{1,i}:$$
$$\boldsymbol{w}_{n,i}^T(\boldsymbol{q})\ddot{\boldsymbol{q}} + \dot{\boldsymbol{w}}_{n,i}^T(\boldsymbol{q})\dot{\boldsymbol{q}} = 0, \tag{B.36}$$
$$\boldsymbol{\lambda}_{t,i} = -\epsilon(\boldsymbol{\zeta}_{t,i}^-)\mu\lambda_{n,i},{}^{1} \tag{B.37}$$

with the jump sets

$$^{0\leftarrow 1}\mathcal{D} = \{\boldsymbol{q}, \boldsymbol{u} \in \mathbb{R}^n \mid h_{n,i} = 0, \ \lambda_{n,i} = 0\}, \tag{B.38}$$
$$^{2\leftarrow 1}\mathcal{D} = \{\boldsymbol{q}, \boldsymbol{u} \in \mathbb{R}^n \mid h_{n,i} = 0, \ ||\boldsymbol{\zeta}_{t,i}|| = 0\}. \tag{B.39}$$

Stick (2):

$$c_{2,i}:$$
$$\boldsymbol{w}_{n,i}^T(\boldsymbol{q})\ddot{\boldsymbol{q}} + \dot{\boldsymbol{w}}_{n,i}^T(\boldsymbol{q})\dot{\boldsymbol{q}} = 0, \tag{B.40}$$
$$\boldsymbol{W}_{t,i}^T(\boldsymbol{q})\ddot{\boldsymbol{q}} + \dot{\boldsymbol{W}}_{t,i}^T(\boldsymbol{q})\dot{\boldsymbol{q}} = 0, \tag{B.41}$$

with the jump sets

$$^{0\leftarrow2}\mathcal{D} = \{\boldsymbol{q}, \boldsymbol{u} \in \mathbb{R}^n \mid h_{n,i} = 0, \ \lambda_{n,i} = 0\}, \tag{B.42}$$

$$^{1\leftarrow2}\mathcal{D} = \{\boldsymbol{q}, \boldsymbol{u} \in \mathbb{R}^n \mid ||\boldsymbol{\lambda}_{t,i}|| = \lambda_{n,i}\}. \tag{B.43}$$

[1]: Because we assume isotropic friction, we can say $\epsilon(\boldsymbol{\zeta}_{t,i}^+) = \epsilon(\boldsymbol{\zeta}_{t,i}^-)$.
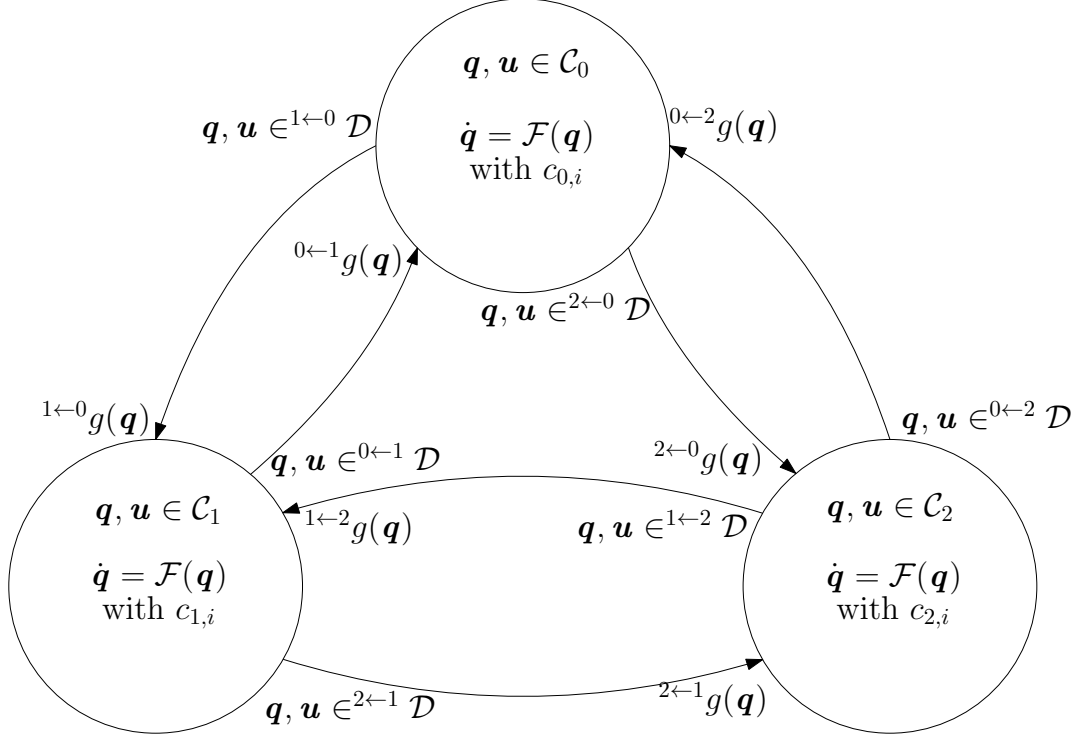

Figure B.2: *The hybrid system representation of one contact point of a system experiencing impact and spatial friction.*

Appendix C

Sensitivity Analysis for Input-Dependent Guards

C.1 Linearization for single jumps

The perturbed state is defined as

$$\boldsymbol{x}(t, \epsilon) = \boldsymbol{x}(t_0, \epsilon) + \int_{t_0}^{t} \boldsymbol{f}(\boldsymbol{x}(s, \epsilon), \boldsymbol{u}(s, \epsilon), s)ds. \tag{C.1}$$

Then

$$\frac{\partial \boldsymbol{x}(t, \epsilon)}{\partial \epsilon} = \frac{\partial \boldsymbol{x}_0}{\partial \epsilon} + \int_{t_0}^{t} \left(\frac{\partial \boldsymbol{f}}{\partial \boldsymbol{x}} \frac{\partial \boldsymbol{x}}{\partial \epsilon} + \frac{\partial \boldsymbol{f}}{\partial \boldsymbol{u}} \frac{\partial \boldsymbol{u}}{\partial \epsilon} \right) ds, \tag{C.2}$$

$$\frac{\partial^2 \boldsymbol{x}}{\partial t \partial \epsilon} = \frac{\partial \boldsymbol{f}}{\partial \boldsymbol{x}} \frac{\partial \boldsymbol{x}}{\partial \epsilon} + \frac{\partial \boldsymbol{f}}{\partial \boldsymbol{u}} \frac{\partial \boldsymbol{u}}{\partial \epsilon}, \tag{C.3}$$

which we can write as

$$\frac{\partial^2 \boldsymbol{x}}{\partial t \partial \epsilon} = D_1 \boldsymbol{f}(\boldsymbol{x}(t, \epsilon), \boldsymbol{u}(t, \epsilon), t) \cdot \frac{\partial \boldsymbol{x}}{\partial \epsilon} + D_2 \boldsymbol{f}(\boldsymbol{x}(t, \epsilon), \boldsymbol{u}(t, \epsilon), t) \cdot \frac{\partial \boldsymbol{u}}{\partial \epsilon}, \tag{C.4}$$

with $D_i \boldsymbol{f}$ the derivative of $\boldsymbol{f}$ wrt the ith term of $\boldsymbol{f}$. Evaluating (C.4) at $\epsilon = 0$ results in the flow dynamics of the positive homogenization

$$\dot{\boldsymbol{z}} = D_1 \boldsymbol{f}(\boldsymbol{\alpha}(t), \boldsymbol{\mu}(t), t) \cdot \boldsymbol{z}(t) + D_2 \boldsymbol{f}(\boldsymbol{\alpha}(t), \boldsymbol{\mu}(t), t) \cdot \boldsymbol{v}(t), \tag{C.5}$$

where

$$\boldsymbol{z}(t) = \frac{\partial \boldsymbol{x}(t, \epsilon)}{\partial \epsilon} \bigg|_{\epsilon=0}, \text{ and } \boldsymbol{v}(t) = \frac{\partial \boldsymbol{u}(t, \epsilon)}{\partial \epsilon} \bigg|_{\epsilon=0}. \tag{C.6}$$

When we consider a single jump

$$\boldsymbol{x}_\epsilon^+(t_\epsilon, \epsilon) = \boldsymbol{g}(\boldsymbol{x}_\epsilon^-(t_\epsilon, \epsilon), t_\epsilon), \tag{C.7}$$

using a Taylor approximation (**Under what conditions is this approximation valid? $\boldsymbol{\gamma}$ continuous, α continuous, $\boldsymbol{f}$ continuous?** with respect to ϵ and around $\epsilon = 0$, we can write

$$\boldsymbol{x}_\epsilon^+(t_\epsilon, \epsilon) = \boldsymbol{\alpha}^+(t_\epsilon) + \epsilon \boldsymbol{z}^+(t_\epsilon) + o(\epsilon), \tag{C.8}$$

$$\boldsymbol{u}_\epsilon^+(t_\epsilon, \epsilon) = \boldsymbol{\mu}^+(t_\epsilon) + \epsilon \boldsymbol{v}^+(t_\epsilon) + o(\epsilon), \tag{C.9}$$

where $\boldsymbol{\alpha}(t)$ is a nominal reference trajectory that satisfies the dynamics of the system and $\boldsymbol{\mu}(t)$ an input that achieves this reference trajectory. Now we expand this in terms of ϵ, so with

$$\Delta = \left.\frac{\partial t_\epsilon}{\partial \epsilon}\right|_{\epsilon=0}, \tag{C.10}$$

we get

$$\boldsymbol{\alpha}^+(t_\epsilon) = \boldsymbol{\alpha}^+(\tau) + \epsilon \dot{\boldsymbol{\alpha}}^+(\tau)\Delta + o(\epsilon), \tag{C.11}$$

$$\boldsymbol{\mu}^+(t_\epsilon) = \boldsymbol{\mu}^+(\tau) + \epsilon \dot{\boldsymbol{\mu}}^+(\tau)\Delta + o(\epsilon), \tag{C.12}$$

$$\boldsymbol{z}^+(t_\epsilon) = \boldsymbol{z}^+(\tau) + \epsilon \dot{\boldsymbol{z}}^+(\tau)\Delta + o(\epsilon), \tag{C.13}$$

$$\boldsymbol{v}^+(t_\epsilon) = \boldsymbol{v}^+(\tau) + \epsilon \dot{\boldsymbol{v}}^+(\tau)\Delta + o(\epsilon), \tag{C.14}$$

which when substituted into (C.8) and (C.9) gives,

$$\boldsymbol{x}_\epsilon^+(t_\epsilon, \epsilon) = \boldsymbol{\alpha}^+(\tau) + \epsilon \dot{\boldsymbol{\alpha}}^+(\tau)\Delta + \epsilon \boldsymbol{z}^+(\tau) + o(\epsilon). \tag{C.15}$$

$$\boldsymbol{u}_\epsilon^+(t_\epsilon, \epsilon) = \boldsymbol{\mu}^+(\tau) + \epsilon \dot{\boldsymbol{\mu}}^+(\tau)\Delta + \epsilon \boldsymbol{v}^+(\tau) + o(\epsilon). \tag{C.16}$$

To find Δ, we evaluate the ante impact guard function

$$\gamma^-(\boldsymbol{x}_\epsilon^-(t_\epsilon), \boldsymbol{u}_\epsilon^-(t_\epsilon), t_\epsilon) = 0. \tag{C.17}$$

In previous work, the guard function γ was not dependent on $\boldsymbol{u}_\epsilon(t_\epsilon)$ because friction and release was not considered. We now expand $\gamma(\boldsymbol{x}_\epsilon(t_\epsilon), \boldsymbol{u}_\epsilon(t_\epsilon), t_\epsilon)$ wrt ϵ, giving

$$\gamma(\boldsymbol{x}_\epsilon(t_\epsilon), \boldsymbol{u}_\epsilon(t_\epsilon), t_\epsilon) = \gamma(\boldsymbol{\alpha}(\tau), \boldsymbol{\mu}(\tau), \tau) + \epsilon \left[\frac{\partial \gamma}{\partial \epsilon}(\boldsymbol{\alpha}(\tau), \boldsymbol{\mu}(\tau), \tau)\right]_{\epsilon=0} + o(\epsilon), \tag{C.18}$$

$$= \gamma(\boldsymbol{\alpha}(\tau), \boldsymbol{\mu}(\tau), \tau) + \epsilon \left[\frac{\partial \gamma}{\partial \boldsymbol{x}}\left(\frac{\partial \boldsymbol{x}}{\partial \epsilon} + \frac{\partial \boldsymbol{x}}{\partial t_\epsilon}\frac{dt_\epsilon}{d\epsilon}\right) + \frac{\partial \gamma}{\partial \boldsymbol{u}}\left(\frac{\partial \boldsymbol{u}}{\partial \epsilon} + \frac{\partial \boldsymbol{u}}{\partial t_\epsilon}\frac{dt_\epsilon}{d\epsilon}\right) + \frac{\partial \gamma}{\partial t_\epsilon}\frac{dt_\epsilon}{d\epsilon}\right]_{\epsilon=0} + o(\epsilon). \tag{C.19}$$

By definition $\gamma(\tau) = 0$, so we can rewrite (C.19) to

$$\gamma(\boldsymbol{x}_\epsilon(t_\epsilon), \boldsymbol{u}_\epsilon(t_\epsilon), t_\epsilon) = \epsilon \left[D_1\gamma \cdot (\overline{\boldsymbol{z}}(\tau) + \dot{\boldsymbol{\alpha}}(\tau)\Delta) + D_2\gamma \cdot (\overline{\boldsymbol{v}}(\tau) + \dot{\boldsymbol{\mu}}(\tau)\Delta) + D_3 \cdot \gamma\Delta\right] \tag{C.20}$$

Now we can evaluate (C.19) using (C.20), which gives

$$\epsilon \left[D_1\gamma^- \cdot (\boldsymbol{z}^-(\tau) + \dot{\boldsymbol{\alpha}}^-(\tau)\Delta) + D_2\gamma^- \cdot (\boldsymbol{v}^-(\tau) + \dot{\boldsymbol{\mu}}^-(\tau)\Delta) + D_3\gamma^- \cdot \Delta\right] = 0. \tag{C.21}$$

From (C.21) we can determine the expression for Δ,

$$\Delta = -\frac{D_1\gamma^- \cdot \boldsymbol{z}^-(\tau) + D_2\gamma^- \cdot \boldsymbol{v}^-(\tau)}{\dot{\gamma}^-}, \tag{C.22}$$

with

$$\gamma^- = \gamma^-(\boldsymbol{\alpha}^-(\tau), \boldsymbol{\mu}^-(\tau), \tau), \tag{C.23}$$

$$\dot{\gamma}^- = D_1\gamma^- \cdot \dot{\boldsymbol{\alpha}}^- + D_2\gamma^- \cdot \dot{\boldsymbol{\mu}}^- + D_3\gamma^-. \tag{C.24}$$

To find the expression for the right hand side of (C.7), we now expand $\boldsymbol{g}(\boldsymbol{x}_\epsilon^-(t_\epsilon, \epsilon), \boldsymbol{u}_\epsilon^-(t_\epsilon, \epsilon), t_\epsilon)$ with respect to ϵ as

$$\boldsymbol{g}(\boldsymbol{x}_\epsilon^-, \boldsymbol{u}_\epsilon^-, t_\epsilon) = \boldsymbol{g}(\boldsymbol{\alpha}^-(\tau), \tau) + \epsilon \left[\frac{\partial \boldsymbol{g}}{\partial \epsilon} \right] + o(\epsilon), \tag{C.25}$$

$$= \boldsymbol{\alpha}^+(\tau) + \epsilon \left[\frac{\partial \boldsymbol{g}}{\partial \boldsymbol{x}} \left(\frac{\partial \boldsymbol{x}}{\partial \epsilon} + \frac{\partial \boldsymbol{x}}{\partial t_\epsilon} \frac{dt_\epsilon}{d\epsilon} \right) + \frac{\partial \boldsymbol{g}}{\partial \boldsymbol{u}} \left(\frac{\partial \boldsymbol{u}}{\partial \epsilon} + \frac{\partial \boldsymbol{u}}{\partial t_\epsilon} \frac{dt_\epsilon}{d\epsilon} \right) + \frac{\partial \boldsymbol{g}}{\partial t_\epsilon} \frac{dt_\epsilon}{d\epsilon} \right]_{\epsilon=0} + o(\epsilon), \tag{C.26}$$

$$= \boldsymbol{\alpha}^+(\tau) + \epsilon \left[D_1\boldsymbol{g} \cdot \left(\boldsymbol{z}^- + \dot{\boldsymbol{\alpha}}^- \Delta \right) + D_2\boldsymbol{g} \cdot \left(\boldsymbol{v}^- + \dot{\boldsymbol{\mu}}(\tau)\Delta \right) + D_3\boldsymbol{g} \cdot \Delta \right] + o(\epsilon). \tag{C.27}$$

Note that $\boldsymbol{g}$ does not depend on the input $\boldsymbol{u}$. Jump maps are impulsive by definition, and since impulsive inputs do not exist it is impossible for the jump map to be dependent on $\boldsymbol{u}$. For small ϵ, we can rewrite (C.7), (C.22) and (C.27) to a general jump map with counter k as

$$\boldsymbol{x}_\epsilon^k(t_\epsilon, \epsilon) = \boldsymbol{g}^k(\boldsymbol{x}_\epsilon^{k-1}, \boldsymbol{u}_\epsilon^{k-1}, t_\epsilon), \tag{C.28}$$

$$\Delta^k = -\frac{D_1\gamma^k \cdot \boldsymbol{z}^{k-1}(\tau) + D_2\gamma^k \cdot \boldsymbol{v}^{k-1}(\tau)}{\dot{\gamma}^k}, \tag{C.29}$$

$$\boldsymbol{g}^k(\boldsymbol{x}_\epsilon^{k-1}, \boldsymbol{u}_\epsilon^{k-1}, t_\epsilon) = \boldsymbol{\alpha}^k(\tau) + \epsilon \left[D_1\boldsymbol{g}^k \cdot \left(\boldsymbol{z}^{k-1}(\tau) + \dot{\boldsymbol{\alpha}}^{k-1}\Delta^k \right) + D_2\boldsymbol{g}^k \cdot \left(\boldsymbol{v}^{k-1}(\tau) + \dot{\boldsymbol{\mu}}^{k-1}\Delta^k \right) + D_3\boldsymbol{g}^k \cdot \Delta^k \right]. \tag{C.30}$$

From (C.15) we get

$$\boldsymbol{z}^k(\tau) = \frac{1}{\epsilon} \left(\boldsymbol{x}_\epsilon^k(t_\epsilon) - \boldsymbol{\alpha}^k(\tau) \right) - \dot{\boldsymbol{\alpha}}^k(\tau)\Delta^k, \tag{C.31}$$

and by equating (C.28) and (C.30) we find an expression for $\overline{\boldsymbol{x}}_\epsilon^k(t_\epsilon, \epsilon)$ which we can substitute into (C.31) resulting in

$$\boldsymbol{z}^k(\tau) = D_1\boldsymbol{g}^k \cdot \left(\boldsymbol{z}^{k-1}(\tau) + \dot{\boldsymbol{\alpha}}^{k-1}\Delta^k \right) + D_2\boldsymbol{g}^k \cdot \left(\boldsymbol{v}^{k-1}(\tau) + \dot{\boldsymbol{\mu}}^{k-1}\Delta^k \right) + D_3\boldsymbol{g}^k \cdot \Delta^k - \dot{\boldsymbol{\alpha}}^k(\tau)\Delta^k. \tag{C.32}$$

Now, by substituting (C.29) into (C.32), we get

$$\boldsymbol{z}^k(\tau) = D_1\boldsymbol{g}^k \cdot \boldsymbol{z}^{k-1} + D_2\boldsymbol{g}^k \cdot \boldsymbol{v}^{k-1}$$
$$- \left(D_1\boldsymbol{g}^k \cdot \boldsymbol{f}^{k-1} + D_2\boldsymbol{g}^k \cdot \dot{\boldsymbol{\mu}}^{k-1} + D_3\boldsymbol{g}^k \cdot 1 - \boldsymbol{f}^k \right) \frac{D_1\gamma^k \cdot \boldsymbol{z}^{k-1} + D_2\gamma^k \cdot \boldsymbol{v}^{k-1}}{\dot{\gamma}^k}, \tag{C.33}$$

$$\boldsymbol{z}^k(\tau) = \left(\frac{\boldsymbol{f}^k - \dot{\boldsymbol{g}}^k}{\dot{\gamma}^k} D_1\gamma^k + D_1\boldsymbol{g}^k \right) \cdot \boldsymbol{z}^{k-1} + \left(\frac{\boldsymbol{f}^k - \dot{\boldsymbol{g}}^k}{\dot{\gamma}^k} D_2\gamma^k + D_2\boldsymbol{g}^k \right) \cdot \boldsymbol{v}^{k-1}, \tag{C.34}$$

with

$$\dot{\boldsymbol{g}}^k = D_1\boldsymbol{g}^k \cdot \boldsymbol{f}^{k-1} + D_2\boldsymbol{g}^k \cdot \dot{\boldsymbol{\mu}}^{k-1} + D_3\boldsymbol{g}^k \cdot 1, \tag{C.35}$$

$$\boldsymbol{f}^k = {}^{s^k}\boldsymbol{f}(\boldsymbol{\alpha}^k(\tau), \boldsymbol{\mu}^k(\tau), \tau). \tag{C.36}$$

Now, using

$$\boldsymbol{G}_{\boldsymbol{z}}^k(\tau) = \frac{\boldsymbol{f}^k - \dot{\boldsymbol{g}}^k}{\dot{\gamma}^k} D_1\gamma^k \cdot 1 + D_1\boldsymbol{g}^k \cdot 1, \tag{C.37}$$

$$\boldsymbol{G}_{\boldsymbol{v}}^k(\tau) = \frac{\boldsymbol{f}^k - \dot{\boldsymbol{g}}^k}{\dot{\gamma}^k} D_2\gamma^k \cdot 1 + D_2\boldsymbol{g}^k \cdot 1, \tag{C.38}$$

we can write

$$z^k(\tau) = G_z^k z^{k-1} + G_v^k v^{k-1}. \tag{C.39}$$

C.2 Linearization for multiple jumps

With $k + 1 = k^+$ and $k - 1 = k^-$, we now assume that we find the first order approximation of the perturbed post-impact state of two simultaneous jumps, by considering these jumps after each other as

$$z^{k^+}(\tau) = G_z^{k^+} z^k + G_v^{k^+} v^k \tag{C.40}$$

$$z^{k^+}(\tau) = G_z^{k^+} \left(G_z^k z^{k^-} + G_v^k v^{k^-} \right) + G_z^{k^+} v^k, \tag{C.41}$$

$$= G_z^{k^+} G_z^k z^{k^-} + G_z^{k^+} G_v^k v^{k^-} + G_v^{k^+} v^k. \tag{C.42}$$

We prove that this is true by deriving an expression for the post-impact state of two simultaneous jumps, and comparing it with (C.42). Now we evaluate the jump map of two jumps at the same time instant τ,

$$^{s^{k^+}\leftarrow s^k \leftarrow s^{k^-}} x_\epsilon(t_\epsilon^{k^+}) = g^{k^+}(x_\epsilon^k(t_\epsilon^{k^+}), u_\epsilon^k(t_\epsilon^{k^+}), t_\epsilon^{k^+}), \tag{C.43}$$

with

$$x_\epsilon^k(t_\epsilon^{k^+}) = \int_{t_\epsilon^k}^{t_\epsilon^{k^+}} \left[{}^{s^k} f\left(x_\epsilon^k(t), u_\epsilon^k(t)\right) \right] dt + g^k(x_\epsilon^{k^-}(t_\epsilon^k), u_\epsilon^{k^-}(t_\epsilon^k), t_\epsilon^k). \tag{C.44}$$

We rewrite the integral in (C.44) to

$$\int_{t_\epsilon^k}^{t_\epsilon^{k^+}} {}^{s^k} f(t, \epsilon) dt = F(t_\epsilon^{k^+}, \epsilon) - F(t_\epsilon^k, \epsilon) = \Phi(t_\epsilon^k, t_\epsilon^{k^+}, \epsilon), \tag{C.45}$$

where ${}^{s^k} f\left(x_\epsilon^k(t), u_\epsilon^k(t)\right)$ can be written as ${}^{s^k} f(t, \epsilon)$, because x_ϵ and u depend solely on t and ϵ. We now expand Φ with respect to ϵ, which results in

$$\Phi(t_\epsilon^k, t_\epsilon^{k^+}, \epsilon) = \Phi(t_0^k, t_0^{k^+}, \epsilon) + \epsilon \left. \frac{\partial \Phi}{\partial \epsilon} \right|_{\epsilon=0} + o(\epsilon), \tag{C.46}$$

$$= F(\tau, 0) - F(\tau, 0) + \left[{}^{s^k} f(t_\epsilon^{k^+}, \epsilon) \frac{dt_\epsilon^{k^+}}{d\epsilon} - {}^{s^k} f(t_\epsilon^{k^+}, \epsilon) \frac{dt_\epsilon^k}{d\epsilon} + \int_{t_\epsilon^k}^{t_\epsilon^{k^+}} \frac{\partial {}^{s^k} f(t, \epsilon)}{\partial \epsilon} dt \right]_{\epsilon=0}, \tag{C.47}$$

$$= f^k(\Delta^{k^+} - \Delta^k), \tag{C.48}$$

since $\int_{t_\epsilon^k}^{t_\epsilon^{k^+}} \frac{\partial {}^{s^k} f(t,\epsilon)}{\partial \epsilon} dt_{\epsilon=0} = 0$. Note that ϵ is assumed sufficiently small, such that we can write t as a function of ϵ.

By expanding (C.43) with respect to ϵ, we find

$$
^{s^{k^+}\leftarrow s^k\leftarrow s^{k^-}}\boldsymbol{x}_\epsilon(t_\epsilon^{k^+}) = \boldsymbol{\alpha}^{k^+}(\tau) + \epsilon \left.\frac{\partial \boldsymbol{g}^{k^+}(\boldsymbol{x}_\epsilon^k(t_\epsilon^{k^+}), \boldsymbol{u}_\epsilon^k(t_\epsilon^{k^+}), t_\epsilon^{k^+})}{\partial \epsilon}\right|_{\epsilon=0} + o(\epsilon), \qquad \text{(C.49)}
$$

where

$$
\left.\frac{\partial \boldsymbol{g}^{k^+}(\boldsymbol{x}_\epsilon^k(t_\epsilon^{k^+}), \boldsymbol{u}_\epsilon^k(t_\epsilon^{k^+}), t_\epsilon^{k^+})}{\partial \epsilon}\right|_{\epsilon=0} = \left[\frac{\partial \boldsymbol{g}^{k^+}}{\partial \boldsymbol{x}}\left(\frac{\partial \boldsymbol{\Phi}}{\partial \epsilon} + \frac{\partial \boldsymbol{g}^k}{\partial \boldsymbol{x}}\left(\frac{\partial \boldsymbol{x}^{k^-}}{\partial \epsilon} + \frac{\partial \boldsymbol{x}^{k^-}}{\partial t}\frac{dt_\epsilon^k}{d\epsilon}\right) + \right.\right.
$$

$$
\left.\left.\frac{\partial \boldsymbol{g}^k}{\partial \boldsymbol{u}}\left(\frac{\partial \boldsymbol{u}^{k^-}}{\partial \epsilon} + \frac{\partial \boldsymbol{u}^{k^-}}{\partial t}\frac{dt_\epsilon^k}{d\epsilon}\right) + \frac{\partial \boldsymbol{g}^k}{\partial t}\frac{dt_\epsilon^k}{d\epsilon}\right) + \frac{\partial \boldsymbol{g}^{k^+}}{\partial t}\frac{dt_\epsilon^{k^+}}{d\epsilon}\right]_{\epsilon=0}, \quad \text{(C.50)}
$$

$$
\left.\frac{\partial \boldsymbol{g}^{k^+}(\boldsymbol{x}_\epsilon^k(t_\epsilon^{k^+}), \boldsymbol{u}_\epsilon^k(t_\epsilon^{k^+}), t_\epsilon^{k^+})}{\partial \epsilon}\right|_{\epsilon=0} = D_1\boldsymbol{g}^{k^+}\cdot\left(\boldsymbol{f}^k(\Delta^{k^+} - \Delta^k) + D_1\boldsymbol{g}^k\cdot\left(\boldsymbol{z}^{k^-} + \boldsymbol{f}^{k^-}\Delta^k\right)\right.
$$

$$
\left. + D_2\boldsymbol{g}^k\cdot\left(\boldsymbol{v}^{k^-} + \dot{\boldsymbol{\mu}}^{k^-}\Delta^k\right) + D_3\boldsymbol{g}^k\cdot\Delta^k\right) + D_3\boldsymbol{g}^{k^+}\cdot\Delta^{k^+}. \quad \text{(C.51)}
$$

We now substitute (C.51) into (C.49), which we in turn substitute into (C.31) to get

$$
\boldsymbol{z}^{k^+}(\tau) = D_1\boldsymbol{g}^{k^+}\cdot\boldsymbol{f}^k\Delta^{k^+} - D_1\boldsymbol{g}^{k^+}\cdot\boldsymbol{f}^{k^+}\Delta^k + D_1\boldsymbol{g}^{k^+}\cdot\left(D_1\boldsymbol{g}^k\cdot\left(\boldsymbol{z}^{k^-} + \boldsymbol{f}^{k^-}\Delta^k\right)\right.
$$

$$
\left. + D_2\boldsymbol{g}^k\cdot\left(\boldsymbol{v}^{k^-} + \dot{\boldsymbol{\mu}}^{k^-}\Delta^k\right) + D_3\boldsymbol{g}^k\cdot\Delta^k\right) + \left(D_3\boldsymbol{g}^{k^+}\cdot 1 - \boldsymbol{f}^{k^+}\right)\Delta^{k^+}, \quad \text{(C.52)}
$$

under the assumption that ϵ is small. The four terms in (C.52) can be rewritten into

$$
D_1\boldsymbol{g}^{k^+}\cdot\boldsymbol{f}^k\Delta^{k^+} = \frac{-D_1\boldsymbol{g}^{k^+}\cdot\boldsymbol{f}^{k^+}}{\dot{\gamma}^{k^+}}\left(D_1\gamma^{k^+}\cdot\left(\boldsymbol{G}_z^k\boldsymbol{z}^{k^-} + \boldsymbol{G}_v^k\boldsymbol{v}^{k^-}\right) + D_2\gamma^{k^+}\cdot\boldsymbol{v}^k\right), \qquad \text{(C.53)}
$$

$$
D_1\boldsymbol{g}^{k^+}\cdot\left(-\boldsymbol{f}^k\Delta^k\right) = \frac{D_1\boldsymbol{g}^{k^+}\cdot\boldsymbol{f}^k}{\dot{\gamma}^k}\left(D_1\gamma^k\cdot\boldsymbol{z}^{k^-} + D_2\gamma^k\cdot\boldsymbol{v}^{k^-}\right), \qquad \text{(C.54)}
$$

$$
D_1\boldsymbol{g}^{k^+}\cdot\left(D_1\boldsymbol{g}^k\cdot\left(\boldsymbol{z}^{k^-} + \boldsymbol{f}^{k^-}\Delta^k\right) + D_2\boldsymbol{g}^k\cdot\left(\boldsymbol{v}^{k^-} + \dot{\boldsymbol{\mu}}^{k^-}\Delta^k\right) + D_3\boldsymbol{g}^k\cdot\Delta^k\right) =
$$

$$
D_1\boldsymbol{g}^{k^+}\cdot\left(\frac{-D_1\boldsymbol{g}^k\cdot\boldsymbol{f}^{k^-}}{\dot{\gamma}^k}D_1\gamma^k + \frac{-D_2\boldsymbol{g}^k\cdot\dot{\boldsymbol{\mu}}^{k^-}}{\dot{\gamma}^k}D_1\gamma^k + \frac{-D_3\boldsymbol{g}^k\cdot 1}{\dot{\gamma}^k}D_1\gamma^k + D_1\boldsymbol{g}^k\right)\cdot\boldsymbol{z}^{k^-}
$$

$$
+ D_1\boldsymbol{g}^{k^+}\cdot\left(\frac{-D_1\boldsymbol{g}^k\cdot\boldsymbol{f}^{k^-}}{\dot{\gamma}^k}D_2\gamma^k + \frac{-D_2\boldsymbol{g}^k\cdot\dot{\boldsymbol{\mu}}^{k^-}}{\dot{\gamma}^k}D_2\gamma^k + \frac{-D_3\boldsymbol{g}^k\cdot 1}{\dot{\gamma}^k}D_2\gamma^k + D_2\boldsymbol{g}^k\right)\cdot\boldsymbol{v}^{k^-}, \quad \text{(C.55)}
$$

$$
\left(D_3\boldsymbol{g}^{k^+}\cdot 1 - \boldsymbol{f}^{k^+}\right)\Delta^{k^+} = \frac{-D_3\boldsymbol{g}^{k^+}\cdot 1 + \boldsymbol{f}^{k^+}}{\dot{\gamma}^{k^+}}\left(D_1\gamma^{k^+}\cdot\left(\boldsymbol{G}_z^k\boldsymbol{z}^{k^-} + \boldsymbol{G}_v^k\boldsymbol{v}^{k^-}\right) + D_2\gamma^{k^+}\cdot\boldsymbol{v}^k\right).
$$

$$
\text{(C.56)}
$$

When we substitute the equations above into (C.52), after reordering the expression we get

---

$$z^{k^+}(\tau) = \left(\frac{\boldsymbol{f}^{k^+} - D_1\boldsymbol{g}^{k^+} \cdot \boldsymbol{f}^k - D_2\boldsymbol{g}^{k^+} \cdot \dot{\boldsymbol{\mu}}^k - D_3\boldsymbol{g}^{k^+} \cdot 1}{\dot{\gamma}^{k^+}} D_1\gamma^{k^+} \cdot \boldsymbol{G}_{\boldsymbol{z}}^k \right.$$

$$\left. + D_1\boldsymbol{g}^{k^+} \cdot \frac{\boldsymbol{f}^k - D_1\boldsymbol{g}^k \cdot \boldsymbol{f}^{k^-} - D_2\boldsymbol{g}^k \cdot \dot{\boldsymbol{\mu}}^{k^-} - D_3\boldsymbol{g}^k \cdot 1}{\dot{\gamma}^k} D_1\gamma^{k^+} + D_1\boldsymbol{g}^{k^+} D_1\boldsymbol{g}^k \cdot 1 \right) \boldsymbol{z}^{k^-}$$

$$+ \left(\frac{\boldsymbol{f}^{k^+} - D_1\boldsymbol{g}^{k^+} \cdot \boldsymbol{f}^k - D_2\boldsymbol{g}^{k^+} \cdot \dot{\boldsymbol{\mu}}^k - D_3\boldsymbol{g}^{k^+} \cdot 1}{\dot{\gamma}^{k^+}} D_1\gamma^{k^+} \cdot \boldsymbol{G}_{\boldsymbol{v}}^k \right.$$

$$\left. + D_1\boldsymbol{g}^{k^+} \cdot \frac{\boldsymbol{f}^k - D_1\boldsymbol{g}^k \cdot \boldsymbol{f}^{k^-} - D_2\boldsymbol{g}^k \cdot \dot{\boldsymbol{\mu}}^{k^-} - D_3\boldsymbol{g}^k \cdot 1}{\dot{\gamma}^k} D_2\gamma^{k^+} + D_1\boldsymbol{g}^{k^+} D_2\boldsymbol{g}^k \cdot 1 \right) \boldsymbol{v}^{k^-}$$

$$+ \left(\frac{\boldsymbol{f}^{k^+} - D_1\boldsymbol{g}^{k^+} \cdot \boldsymbol{f}^k - D_2\boldsymbol{g}^{k^+} \cdot \dot{\boldsymbol{\mu}}^k - D_3\boldsymbol{g}^{k^+} \cdot 1}{\dot{\gamma}^{k^+}} D_2\gamma^{k^+} \right) \boldsymbol{v}^k, \quad \text{(C.57)}$$

from which we can isolate $\boldsymbol{G}_{\boldsymbol{z}}^k$, and $\boldsymbol{G}_{\boldsymbol{v}}^k$ resulting in

$$z^{k^+}(\tau) = \left(\frac{\boldsymbol{f}^{k^+} - D_1\boldsymbol{g}^{k^+} \cdot \boldsymbol{f}^k - D_2\boldsymbol{g}^{k^+} \cdot \dot{\boldsymbol{\mu}}^k - D_3\boldsymbol{g}^{k^+} \cdot 1}{\dot{\gamma}^{k^+}} D_1\gamma^{k^+} + D_1\boldsymbol{g}^{k^+} \cdot 1 \right) \boldsymbol{G}_{\boldsymbol{z}}^k \boldsymbol{z}^{k^-}$$

$$+ \left(\frac{\boldsymbol{f}^{k^+} - D_1\boldsymbol{g}^{k^+} \cdot \boldsymbol{f}^k - D_2\boldsymbol{g}^{k^+} \cdot \dot{\boldsymbol{\mu}}^k - D_3\boldsymbol{g}^{k^+} \cdot 1}{\dot{\gamma}^{k^+}} D_1\gamma^{k^+} + D_1\boldsymbol{g}^{k^+} \cdot 1 \right) \boldsymbol{G}_{\boldsymbol{v}}^k \boldsymbol{v}^{k^-}$$

$$+ \left(\frac{\boldsymbol{f}^{k^+} - D_1\boldsymbol{g}^{k^+} \cdot \boldsymbol{f}^k - D_2\boldsymbol{g}^{k^+} \cdot \dot{\boldsymbol{\mu}}^k - D_3\boldsymbol{g}^{k^+} \cdot 1}{\dot{\gamma}^{k^+}} D_2\gamma^{k^+} \right) \boldsymbol{v}^k, \quad \text{(C.58)}$$

which is equal to

$$z^{k^+}(\tau) = \boldsymbol{G}_{\boldsymbol{z}}^{k^+} \boldsymbol{G}_{\boldsymbol{z}}^k \boldsymbol{z}^{k^-} + \boldsymbol{G}_{\boldsymbol{z}}^{k^+} \boldsymbol{G}_{\boldsymbol{v}}^k \boldsymbol{v}^{k^-} + \boldsymbol{G}_{\boldsymbol{v}}^{k^+} \boldsymbol{v}^k. \quad \text{(C.59)}$$

Here we see that (C.59) is equal to (C.42). This proves that for any k, the first-order approximation of the post-impact state of two simultaneous jumps at τ can be found by evaluating the two jumps separately. Since k is a variable in this proof, using an induction-like proof, this holds for any amount of jumps as well. This is illustrated in Figure C.1.
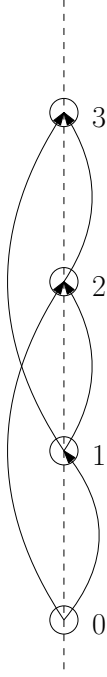
Figure C.1

When we take $k = 1$, we show that the jumps from 0 to 2 can be described by evaluating the jump from 0 to 1 and the jump 1 to 2 in succession. This also holds for $k = 2$. The jump from 0 to 3 can be described by evaluating the jump from 0 to 2 and the jump from 2 to 3 in succession. This way we proved that we can use (C.59) to find an expression for the first-order approximation of the post-impact state for l simultaneous jumps, with $l \in \mathbb{Z}$. Also, we show that multiple constant jump gains will result in a total jump which can also be described by a constant jump gain.

For l simultaneous jumps, we can find the first-order approximation of the post-impact state using

$$^{l \leftarrow 0}\boldsymbol{z}(\tau) = {}^{l \leftarrow 0}\boldsymbol{G}(\boldsymbol{z}^0(\tau), \boldsymbol{v}(\tau), \tau) = {}^{l \leftarrow 0}\boldsymbol{G}_{\boldsymbol{z}}\boldsymbol{z}^0(\tau) + \sum_{i=0}^{l-1} \left({}^{l \leftarrow i+1}\boldsymbol{G}_{\boldsymbol{z}} {}^{i+1 \leftarrow i}\boldsymbol{G}_{\boldsymbol{v}}\boldsymbol{v}^i(\tau) \right), \qquad \text{(C.60)}$$

where the superscript

$$b \leftarrow a = b \leftarrow (b-1) \leftarrow \cdots \leftarrow (a+1) \leftarrow a, \qquad \text{(C.61)}$$

and

$$^{b \leftarrow a}\boldsymbol{G}_{\boldsymbol{z}} = {}^{b \leftarrow (b-1)}\boldsymbol{G}_{\boldsymbol{z}} \cdots {}^{(a+2) \leftarrow (a+1)}\boldsymbol{G}_{\boldsymbol{z}}^{(a+1) \leftarrow a}\boldsymbol{G}_{\boldsymbol{z}}, \qquad \text{(C.62)}$$

$$^{b \leftarrow a}\boldsymbol{G}_{\boldsymbol{v}} = {}^{b \leftarrow (b-1)}\boldsymbol{G}_{\boldsymbol{v}} \cdots {}^{(a+2) \leftarrow (a+1)}\boldsymbol{G}_{\boldsymbol{v}}^{(a+1) \leftarrow a}\boldsymbol{G}_{\boldsymbol{v}}. \qquad \text{(C.63)}$$

Appendix D

Positive Homogenization for Input-Dependent Guards

D.1 Conewise constant jump gain

This section is written under the assumption that in one macro event, only two modes are possible per contact point. The general form of a jump map for simultaneous impacts with is

$$
{}^{s^l \leftarrow s^0} \boldsymbol{z}(\tau) = {}^{s^l \leftarrow s^0} \boldsymbol{H}(\boldsymbol{z}^0(\tau), \boldsymbol{v}(\tau), \tau) = \begin{cases} \boldsymbol{G}^1(\boldsymbol{z}^0, \boldsymbol{v}^0, \tau), & \text{if condition 1 is true,} \\ \boldsymbol{G}^2(\boldsymbol{z}^0, \boldsymbol{v}^0, \tau), & \text{if condition 1 is true,} \\ \vdots & \vdots \\ \boldsymbol{G}^{p^{c_i}}(\boldsymbol{z}^0, \boldsymbol{v}^0, \tau), & \text{if condition } p^{c_i} \text{ is true,} \end{cases} \tag{D.1}
$$

where $\boldsymbol{G}$ is in the form of (C.60). We will now derive the jump maps and associated conditions in (D.1) to make the expression explicit.

During a macro event for a certain perturbation, only a single order of micro events is feasible. This order can be found by determining the perturbed jump time of all possible micro events, and selecting the micro event with the earliest impact time as the next event. Mathematically, this is written as

$$
s^{k+1} = \underset{s^{k+1}}{\arg\min} \left({}^{s^{k+1} \leftarrow S^k} t_\epsilon \right). \tag{D.2}
$$

The impact time of the next micro event ${}^{s^{k+1} \leftarrow S^k} t_\epsilon$ can be approximated using the first order approximation

$$
{}^{s^{k+1} \leftarrow S^k} t_\epsilon = \tau + \epsilon \Delta^{k+1}. \tag{D.3}
$$

Now, since τ and ϵ are equal for each impact time, we can rewrite (D.2) to

$$
s^{k+1} = \underset{s^{k+1}}{\arg\min} \left(\Delta^{k+1} \right), \tag{D.4}
$$

which can be written as

$$
s^{k+1} = s^k + \underset{\eta^* \in \chi}{\arg\min} \left(-\frac{D_1 \gamma^{\eta^*} \left({}^{s^k}\alpha, {}^{s^k}\mu, \tau \right) {}^{S^k}\overline{\boldsymbol{z}} + D_2 \gamma^{\eta^*} \left({}^{s^k}\alpha, {}^{s^k}\mu, \tau \right) {}^{S^k}\overline{\boldsymbol{v}}}{\dot{\gamma}^{\eta^*}} \right), \tag{D.5}
$$

with χ the set of guard identifiers that are still open. Then

$$\eta^{k+1} = \underset{\eta^* \in \chi}{\operatorname{argmin}} \left(-\frac{D_1 \gamma^{\eta^*} \left({}^{s^k}\alpha, {}^{s^k}\mu, \tau \right) {}^{S^k}\overline{z} + D_2 \gamma^{\eta^*} \left({}^{s^k}\alpha, {}^{s^k}\mu, \tau \right) {}^{S^k}\overline{v}}{\dot{\gamma}^{\eta^*}} \right), \tag{D.6}$$

with $s^{k+1} = s^k + \eta^{k+1}$ and η^{k+1} a guard function identifier. Finally, with

$$^{S^k}a = -\frac{D_1 \gamma^\eta \left({}^{S^k}\alpha, {}^{s^k}\mu, \tau \right)}{\dot{\gamma}^\eta}, \quad {}^{S^k}b = -\frac{D_2 \gamma^\eta \left({}^{S^k}\alpha, {}^{s^k}\mu, \tau \right)}{\dot{\gamma}^\eta}, \tag{D.7}$$

(D.6) can be rewritten as

$$\eta^{k+1} = \underset{\eta^* \in \chi}{\operatorname{argmin}} \left({}^{S^k}a^T \; {}^{S^k}\overline{z} + {}^{s^k}b^T \; {}^{S^k}\overline{v} \right). \tag{D.8}$$

Now, by checking (D.6) for every micro event, we know which jump gains we should take to substitute into (C.60). For example a system with $c_i = 2$ and $p = 3$, with a macro event starting in $s_0 = 00$ and ending in $s_l = 22$, this gives

$$^{S^{2\leftarrow 0}}H({}^{s^0}z(\tau), {}^{S^2}v(\tau), \tau) =$$
$$\begin{cases} {}^{(12)}S^{2\leftarrow 0}G_z \; {}^{s^0}z + {}^{(12)}S^{2\leftarrow 0}G_v \; {}^{s^0}v, & \text{if (I)}, \\ {}^{12}S^{2\leftarrow 1}G_z \; {}^{1}S^{1\leftarrow 0}G_z \; {}^{s^0}z + {}^{12}S^{2\leftarrow 1}G_z \; {}^{1}S^{1\leftarrow 0}G_v \; {}^{s^0}v + {}^{12}S^{2\leftarrow 1}G_v \; {}^{1}S^{1}v, & \text{if (II)}, \\ {}^{21}S^{2\leftarrow 1}G_z \; {}^{2}S^{1\leftarrow 0}G_z \; {}^{s^0}z + {}^{21}S^{2\leftarrow 1}G_z \; {}^{2}S^{1\leftarrow 0}G_v \; {}^{s^0}v + {}^{21}S^{2\leftarrow 1}G_v \; {}^{2}S^{1}v, & \text{if (III)}, \end{cases} \tag{D.9}$$

with

$$(\text{I}) : \; {}^{2}S^1 a^T \; {}^{2}S^1 z + {}^{2}S^1 b^T \; {}^{2}S^1 v = {}^{1}S^1 a^T \; {}^{1}S^1 z + {}^{1}S^1 b^T \; {}^{1}S^1 v, \tag{D.10}$$

$$(\text{II}) : \; {}^{2}S^1 a^T \; {}^{2}S^1 z + {}^{2}S^1 b^T \; {}^{2}S^1 v > {}^{1}S^1 a^T \; {}^{1}S^1 z + {}^{1}S^1 b^T \; {}^{1}S^1 v, \tag{D.11}$$

$$(\text{III}) : \; {}^{2}S^1 a^T \; {}^{2}S^1 z + {}^{2}S^1 b^T \; {}^{2}S^1 v < {}^{1}S^1 a^T \; {}^{1}S^1 z + {}^{1}S^1 b^T \; {}^{1}S^1 v. \tag{D.12}$$

These conditions are illustrated in Figure D.1. Since the conditions are linear in z and v, they appear as lines in the state space of z and v. When we introduce more conditions, we will find several cones that relate a certain jump gain to z, v pair. When we look at the vector $r(z, v)$ in Figure D.1, we notice that when r is multiplied with a constant α we will always stay in the same cone, i.e. use the same jump gain. Hence the name, conewise constant jump gain.
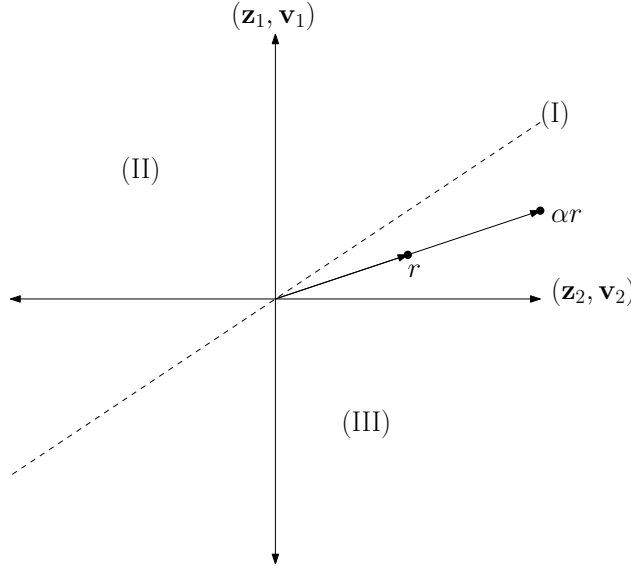
Figure D.1

D.2 Positive homogeneity

The first order approximation of the perturbed trajectory $\boldsymbol{x}_\epsilon$ can be found using $\boldsymbol{\alpha} + \epsilon \boldsymbol{z}$, with

$$
\begin{aligned}
{}^{s^{k-1}}\dot{\boldsymbol{z}} &= {}^{s^{k-1}}\boldsymbol{A}(t)\ {}^{s^{k-1}}\boldsymbol{z} + {}^{s^{k-1}}\boldsymbol{B}(t)\ {}^{s^{k-1}}\boldsymbol{v}, \\
{}^{s^{k}}\boldsymbol{z} &= {}^{s^{k} \leftarrow s_{k-1}}\boldsymbol{H}\left({}^{s^{k-1}}\boldsymbol{z}, t \right), \\
{}^{s^{k}}\dot{\boldsymbol{z}} &= {}^{s^{k}}\boldsymbol{A}(t)\ {}^{s^{k}}\boldsymbol{z} + {}^{s^{k}}\boldsymbol{B}(t)\ {}^{s^{k-1}}\boldsymbol{v},
\end{aligned}
\tag{D.13}
$$

where

$$
{}^{s^{k}}\boldsymbol{A}(t) = D_1\ {}^{s^{k}}\boldsymbol{f}\left({}^{s^{k}}\boldsymbol{\alpha}(t),\ {}^{s^{k}}\boldsymbol{\mu}(t) \right),
\tag{D.14}
$$

$$
{}^{s^{k}}\boldsymbol{B}(t) = D_2\ {}^{s^{k}}\boldsymbol{f}\left({}^{s^{k}}\boldsymbol{\alpha}(t),\ {}^{s^{k}}\boldsymbol{\mu}(t) \right).
\tag{D.15}
$$

When we look at (D.13), the continuous dynamics of the system are linear. Because of the conewise constant jump gain however, this linearity property is lost. We can see this by looking at the general solution of (D.13). A system $f(x, u)$ with state x and input u is linear if $f(x_1, v_1) + f(x_2, v_2) = f(x_1 + x_2, v_1 + v_2)$. Two solutions of (D.13) before jump are

$$
{}^{s^{k-1}}\boldsymbol{z}_1(\tau) = {}^{s^{k-1}}\boldsymbol{\phi}(t, t_0)\ {}^{s^{k-1}}\boldsymbol{z}_1(t_0) + \int_{t_0}^{\tau} \left[{}^{s^{k-1}}\boldsymbol{\phi}(t, s)\ {}^{s^{k-1}}\boldsymbol{B}(s)\boldsymbol{v}_1(s) \right] ds,
\tag{D.16}
$$

$$
{}^{s^{k-1}}\boldsymbol{z}_2(\tau) = {}^{s^{k-1}}\boldsymbol{\phi}(t, t_0)\ {}^{s^{k-1}}\boldsymbol{z}_2(t_0) + \int_{t_0}^{\tau} \left[{}^{s^{k-1}}\boldsymbol{\phi}(t, s)\ {}^{s^{k-1}}\boldsymbol{B}(s)\boldsymbol{v}_2(s) \right] ds,
\tag{D.17}
$$

with t_0 the initial time and τ the jump time. When we add these solutions together we find

$$
\begin{aligned}
{}^{s^{k-1}}\boldsymbol{z}_1(\tau) + {}^{s^{k-1}}\boldsymbol{z}_2(\tau) = {}^{s^{k-1}}\boldsymbol{\phi}(t, t_0) &\left({}^{s^{k-1}}\boldsymbol{z}_1(t_0) + {}^{s^{k-1}}\boldsymbol{z}_2(t_0) \right) \\
&+ \int_{t_0}^{\tau} \left[{}^{s^{k-1}}\boldsymbol{\phi}(t, s)\ {}^{s^{k-1}}\boldsymbol{B}(s) \left(\boldsymbol{v}_1(s) + \boldsymbol{v}_2(s) \right) \right] ds,
\end{aligned}
\tag{D.18}
$$

---

which is equal to the solution of $^{s^{k-1}}z_3(t_0) =^{s^{k-1}} z_1(t_0) +^{s^{k-1}} z_2(t_0)$ with $v_3(t) = v_1(t) + v_2(t)$. When $^{s^{k-1}}z_1$ jumps with $G^1(z, \tau)$ and $^{s^{k-1}}z_1(\tau)$ jumps with $G^2(z, \tau)$ we find the solutions post jump to be

$$^{s^k}z_1(\tau) = \,^{s^k}\phi(t, t_0) \, G^1(^{s^{k-1}}z_1(t_0), \tau) + \int_{t_0}^{\tau} \left[\,^{s^k}\phi(t, s) \,^{s^k}B(s)v_1(s) \right] ds, \qquad (D.19)$$

$$^{s^k}z_2(\tau) = \,^{s^k}\phi(t, t_0) \, G^2(^{s^{k-1}}z_2(t_0), \tau) + \int_{t_0}^{\tau} \left[\,^{s^k}\phi(t, s) \,^{s^k}B(s)v_2(s) \right] ds, \qquad (D.20)$$

which when added together results in

$$^{s^k}z_1(\tau) + \,^{s^k}z_2(\tau) = \,^{s^k}\phi(t, t_0) \left(G_z^1 \,^{s^{k-1}}z_1 + G_v^1 \,^{s^{k-1}}v_1 + G_z^2 \,^{s^{k-1}}z_2 + G_v^2 \,^{s^{k-1}}v_2 \right)$$
$$+ \int_{t_0}^{\tau} \left[\,^{s^k}\phi(t, s) \,^{s^k}B(s) \left(v_1(s) + v_2(s) \right) \right] ds. \quad (D.21)$$

Here we see that the solution of $^{s^{k-1}}z_3(t_0) =^{s^{k-1}} z_1(t_0) +^{s^{k-1}} z_2(t_0)$ with $v_3(t) = v_1(t) + v_2(t)$, which jumps with $G_3(z, \tau)$, is only the equal to (D.21) if $G_1(z, \tau) = G_2(z, \tau) = G_3(z, \tau)$. In other words, the system only maintains its linearity after jump if the jump maps are equal for each ante jump state. Because this is generally not true, we show that the system is positive homogeneous for any jump gains. A system $f(x, u)$ with state x and input u is called positive homogeneous, when $\alpha f(x, u) = f(\alpha x, \alpha u)$. If we multiply (D.19) with a constant α, we find

$$^{s^k}z_1(\tau) = \alpha \,^{s^k}\phi(t, t_0) \left(G_z^1 \,^{s^{k-1}}z_1 + G_v^1 \,^{s^{k-1}}v_1 \right) + \alpha \int_{t_0}^{\tau} \left[\,^{s^k}\phi(t, s) \,^{s^{k-1}}B(s)v_1(s) \right] ds. \quad (D.22)$$

If we now look at the solution for $z_4(t_0) = \alpha z_1(t_0)$ with $v_4(t) = \alpha v_1(t)$ jumping with $G^4(\tau)$, and using the fact that $G^4(\tau) = G^1(\tau)$ since the gains are conewise constant as illustrated in Figure D.1, we find the same solution as (D.22). This shows that (D.13) is positive homogeneous for any conewise constant jump gain $^{s^k \leftarrow s^{k-1}}H\left(^{s^{k-1}}z, t\right)$. Hence the name, positive homogenization.

D.3 Friction in Mechanical Systems with Unilateral Constraints

D.3.1 Frictional impacts

- It is possible for a contact point when it goes from open to stick to immediately go to slip, through input or for example gravity. Is this a simultaneous event? Also, write proof that there exists a range of epsilon such that an impact away from this event will not cause it to happen.

- How does transversality wrt Γ translate to the behaviour in flow?

- Are the contacts non-superfluous?

- Are the reset maps associative?

D.3.2 Impacts away from slip-stick border

Now we look at the case where a contact point goes from open to closed, away from $\Gamma = 0$. This is illustrated in Figure D.1. The goal is to proof that for an event away from Γ, an infinitesimally

small perturbation can not cause the trajectory to hit $\gamma = 0$ at a perturbed ante-impact state $\boldsymbol{x}_\epsilon^-(t_\epsilon)$ where $\boldsymbol{\Gamma}$ changes sign in comparison with the unperturbed ante-impact state $\boldsymbol{\alpha}^-(\tau)$. From [49, p. 6] we know that based on the continuity property of $\boldsymbol{\gamma}$ and $\boldsymbol{f}$, the perturbed impact state can be written as

$$\boldsymbol{x}_\epsilon(t_\epsilon) = \boldsymbol{\alpha}(\tau) + \epsilon\dot{\boldsymbol{\alpha}}(\tau)\frac{\partial t_\epsilon}{\partial \epsilon} + \epsilon\boldsymbol{z}(\tau) + o(\epsilon), \tag{D.23}$$

for sufficiently small ϵ. The shortest distance between $\boldsymbol{\Gamma} = \boldsymbol{\Gamma}(\boldsymbol{\alpha}(\tau))$ and $\boldsymbol{\Gamma} = 0$ on the plane where $\boldsymbol{\gamma} = 0$ is defined as the constant $\delta_{\boldsymbol{\Gamma}}$, which is also illustrated in Figure D.1.
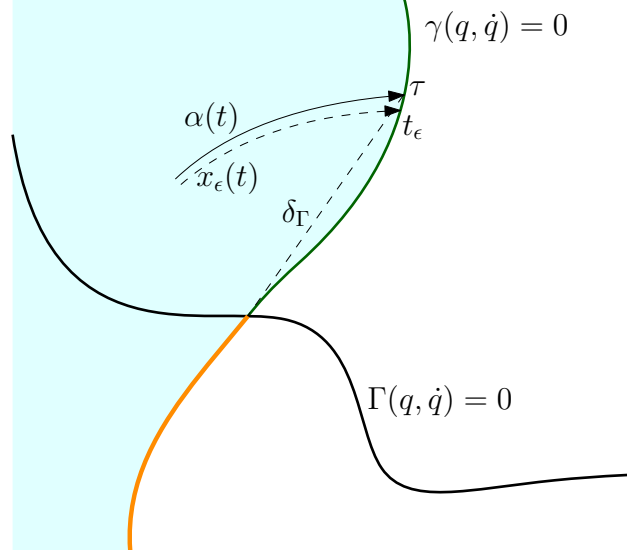
Figure D.1: *The guard functions $\boldsymbol{\gamma}$ and $\boldsymbol{\Gamma}$ in the state space of $\boldsymbol{q}$. A transition from open to closed is made away from $\boldsymbol{\Gamma}$. $\boldsymbol{\alpha}(t)$ is the nominal trajectory and $\boldsymbol{x}_\epsilon(t)$ a perturbed trajectory of the contact point up to the transition.*

Let's define a point in the state $\boldsymbol{x}_{\boldsymbol{\gamma}=0,\boldsymbol{\Gamma}=0}$ where $\boldsymbol{\gamma}(\boldsymbol{x}_{\boldsymbol{\gamma}=0,\boldsymbol{\Gamma}=0}) = 0$ and $\boldsymbol{\Gamma}(\boldsymbol{x}_{\boldsymbol{\gamma}=0,\boldsymbol{\Gamma}=0}) = 0$. We are evaluating nominal trajectories which impact away from $\boldsymbol{\Gamma} = 0$, i.e. $\boldsymbol{\Gamma}(\boldsymbol{\alpha}(\tau)) \neq \boldsymbol{\Gamma}(\boldsymbol{x}_{\boldsymbol{\gamma}=0,\boldsymbol{\Gamma}=0})$. From Section B.3.2 we know that $\boldsymbol{\Gamma}$ is continuously differentiable, which implies that it is Lipschitz-continuous and therefore satisfies the Lipschitz-continuity condition

$$||\boldsymbol{f}(\boldsymbol{x}) - \boldsymbol{f}(\boldsymbol{y})|| \leq \kappa||\boldsymbol{x} - \boldsymbol{y}||, \quad \forall \boldsymbol{x}, \boldsymbol{y} \in \mathbb{R}^n, \tag{D.24}$$

where $\kappa > 0$ [19]. By applying (D.24) to the function value of $\boldsymbol{\Gamma}$ at impact for the nominal trajectory and the perturbed trajectory, we find

$$||\boldsymbol{\Gamma}(\boldsymbol{\alpha}(\tau)) - \boldsymbol{\Gamma}(\boldsymbol{x}_\epsilon(t_\epsilon))|| \leq \kappa||\boldsymbol{\alpha}(\tau) - \boldsymbol{x}_\epsilon(t_\epsilon))||. \tag{D.25}$$

After substituting (D.23) into (D.25), this can be written as

$$||\boldsymbol{\Gamma}(\boldsymbol{\alpha}(\tau)) - \boldsymbol{\Gamma}(\boldsymbol{x}_\epsilon(t_\epsilon))|| \leq \kappa||\epsilon\left(\dot{\boldsymbol{\alpha}}(\tau)\frac{\partial t_\epsilon}{\partial \epsilon} + \boldsymbol{z}(\tau)\right) + o(\epsilon). \tag{D.26}$$

(D.26) shows that $\lim_{\epsilon \to 0} ||\mathbf{\Gamma}(\boldsymbol{\alpha}(\tau)) - \mathbf{\Gamma}(\boldsymbol{x}_\epsilon(t_\epsilon))|| = 0$. Since $\delta_{\mathbf{\Gamma}} > 0$, this proves that for an infinitesimally small perturbation ϵ, $||\mathbf{\Gamma}(\boldsymbol{\alpha}(\tau)) - \mathbf{\Gamma}(\boldsymbol{x}_\epsilon(t_\epsilon))|| < \delta_{\mathbf{\Gamma}}$. It also shows that there always exists a range of ϵ where $||\mathbf{\Gamma}(\boldsymbol{\alpha}(\tau)) - \mathbf{\Gamma}(\boldsymbol{x}_\epsilon(t_\epsilon))|| < \delta_{\mathbf{\Gamma}}$ holds, i.e., there always exists a range of ϵ such that the perturbation will not cause the contact point to switch stick-slip domain at impact in comparison to the unperturbed event.

D.3.3 Impacts close to slip-stick border

- Consider as simultaneous trigger of open-closed guard and slip-stick guard. However, it is not entirely the same, as the slip-stick guard can not be triggered before the open-closed guard.

- The trigger should be transversal, in both closed-open guard and slip-stick guard.

- If we can show continuity of post-impact state, then we can define a jump gain like H, which uses one jump map for the open to stick domain and another jump map for the open to slip domain.

D.3.4 Slip-stick transition in closed-contact

Appendix E

Assumptions on Guard-Activations

E.1 Transversality

E.2 Superfluous Contacts

E.3 Nominal Guard-Activations

For impacts, the theory is valid for impacts away from a simultaneous impacts and for simultaneous impacts, but not for impacts very close to simultaneous impacts. In this case the nominal impact is not a simultaneous impact, but a perturbation can cause the order of impacts to change. I believe the jump gain is not conewise constant anymore in this case.

The same is true for impacts close to the border of stick and slip.

Appendix F

Plank-Box Model

F.1 Plank box dynamics

In Figure F.1 the plank-box model is illustrated. The block is fully actuated and the plank is attached to the solid environment with a spring and damper. The line contact is for now modeled using two contact-points C_L and C_R.
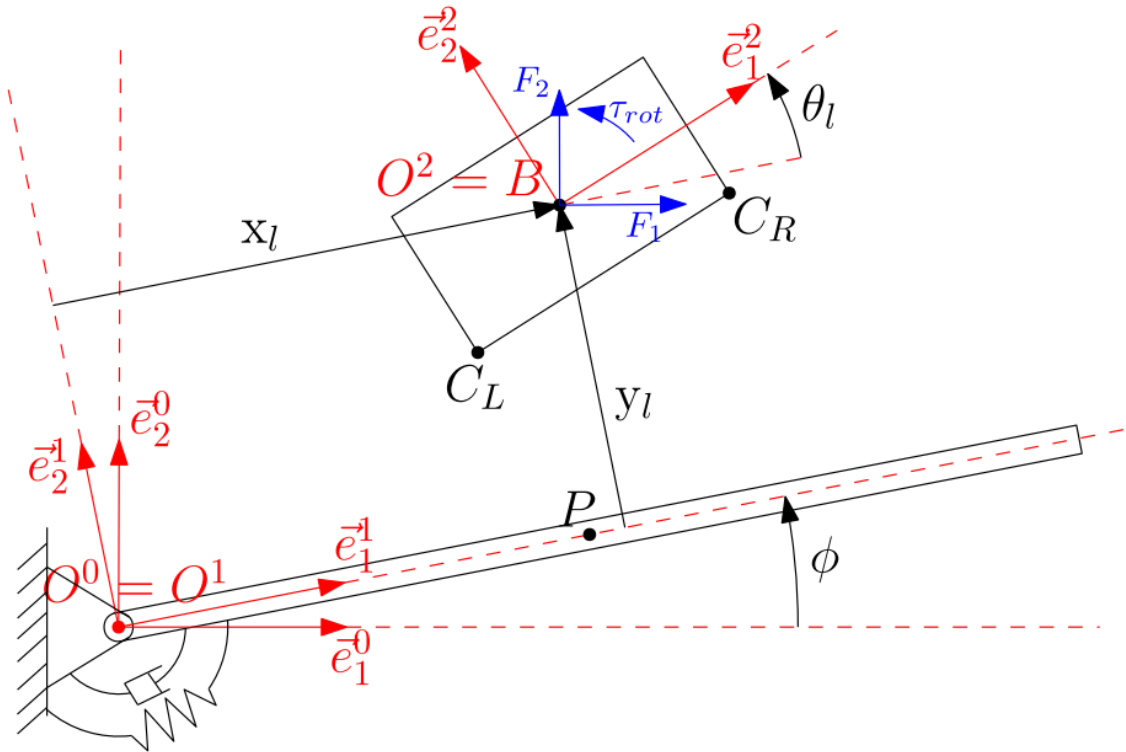

Figure F.1: *Block-plank model*

Global unconstrained dynamics

The global generalized coordinates are defined as

$$q_g = \begin{bmatrix} x_g & y_g & \theta_g & \varphi \end{bmatrix}, \tag{F.1}$$

$$v_g = \begin{bmatrix} \dot{x}_g & \dot{y}_g & \dot{\theta}_g & \dot{\varphi} \end{bmatrix}. \tag{F.2}$$

The equations of motion for the global unconstrained dynamics are then described by

$$\boldsymbol{M}_g(\boldsymbol{q}_g)\dot{\boldsymbol{v}}_g - \boldsymbol{H}_g(\boldsymbol{q}_g, \boldsymbol{v}_g) = \boldsymbol{S}_g(\boldsymbol{q}_g)\boldsymbol{u}, \tag{F.3}$$

with

$$\boldsymbol{M}_g(\boldsymbol{q}_g) = \begin{bmatrix} m_B & 0 & 0 & 0 \\ 0 & m_B & 0 & 0 \\ 0 & 0 & J_B & 0 \\ 0 & 0 & 0 & \frac{m_P L_p{}^2}{4} + J_P \end{bmatrix} \tag{F.4}$$

$$\boldsymbol{H}_g(\boldsymbol{q}_g, \boldsymbol{v}_g) = \begin{bmatrix} 0 \\ -gm_B \\ 0 \\ k_P\varphi - b_P\dot{\varphi} - \frac{L_p g m_P \cos(\varphi)}{2} \end{bmatrix} \tag{F.5}$$

$$\boldsymbol{S}_g(\boldsymbol{q}_g) = \begin{bmatrix} 1 & 0 & 0 \\ 0 & 1 & 0 \\ 0 & 0 & 1 \\ 0 & 0 & 0 \end{bmatrix}. \tag{F.6}$$

Local unconstrained dynamics

The global generalized coordinates $\boldsymbol{q}_g$ can be rewritten to a set of local coordinates $\boldsymbol{q}_l$. In the plank box case they are related via

$$\boldsymbol{q}_g(\boldsymbol{q}_l) = \begin{bmatrix} \cos(\varphi)x_l - \sin(\varphi)y_l \\ \sin(\varphi)x_l + \cos(\varphi)y_l \\ \theta_l + \varphi \\ \varphi \end{bmatrix}. \tag{F.7}$$

The local unconstrained equations of motion are then defined as

$$\boldsymbol{M}_l(\boldsymbol{q}_l)\dot{\boldsymbol{v}}_l - \boldsymbol{H}_l(\boldsymbol{q}_l, \boldsymbol{v}_l) = \boldsymbol{S}_l(\boldsymbol{q}_l)\boldsymbol{u}, \tag{F.8}$$

with

$$
\boldsymbol{M}_l(\boldsymbol{q}_l) = \begin{bmatrix} m_B & 0 & 0 & -m_B y_l \\ 0 & m_B & 0 & m_B x_l \\ 0 & 0 & J_B & J_B \\ -m_B y_l & m_B x_l & J_B & \frac{m_P L_p{}^2}{4} + m_B x_l{}^2 + m_B y_l{}^2 + J_B + J_P \end{bmatrix}
\tag{F.9}
$$

$$
\boldsymbol{H}_l(\boldsymbol{q}_l, \boldsymbol{v}_l) = \begin{bmatrix} m_B \left(x_l \dot{\varphi}^2 + 2\dot{y}_l \dot{\varphi} - g\sin(\varphi) \right) \\ -m_B \left(-y_l \dot{\varphi}^2 + 2\dot{x}_l \dot{\varphi} + g\cos(\varphi) \right) \\ 0 \\ k_P \varphi - b_P \dot{\varphi} - 2m_B \dot{\varphi} x_l \dot{x}_l - 2m_B \dot{\varphi} y_l \dot{y}_l - \frac{L_p g m_P \cos(\varphi)}{2} - g m_B x_l \cos(\varphi) + g m_B y_l \sin(\varphi) \end{bmatrix}
\tag{F.10}
$$

$$
\boldsymbol{S}_l(\boldsymbol{q}_l) = \begin{bmatrix} \cos(\varphi) & \sin(\varphi) & 0 \\ -\sin(\varphi) & \cos(\varphi) & 0 \\ 0 & 0 & 1 \\ -y_l \cos(\varphi) - x_l \sin(\varphi) & x_l \cos(\varphi) - y_l \sin(\varphi) & 1 \end{bmatrix}.
\tag{F.11}
$$

Local constrained dynamics

First we have to determine the position vectors of the points C_L and C_R using Figure F.2. First we define the position vector of C_R,

$$
r_{C_R} = r_B + r_{BC_R} \text{ with,}
\tag{F.12}
$$

$$
r_B = \begin{bmatrix} x_l & y_l & 0 \end{bmatrix} \vec{e}^{\,1},
\tag{F.13}
$$

$$
r_{BC_R} = \begin{bmatrix} BH & HC_R & 0 \end{bmatrix} \vec{e}^{\,1},
\tag{F.14}
$$

using the axis systems defined in the report of Hao. From Figure F.2 and that $\triangle BFG \cong \triangle C_R HG$ we can say

$$
HC_R = \cos(\theta_l) C_R G,
\tag{F.15}
$$

$$
C_R G = FG - FC_R,
\tag{F.16}
$$

$$
FG = \tan(\theta_l) BF,
\tag{F.17}
$$

and with $FC_R = \frac{l_B}{2}$ and $BF = \frac{L_B}{2}$ we find

$$
HC_R = \sin(\theta_l)\frac{L_B}{2} - \cos(\theta_l)\frac{l_B}{2}.
\tag{F.18}
$$

For BH we say

$$
BH = BG - HG,
\tag{F.19}
$$

$$
BG = \frac{1}{\sin(\theta_l)} FG,
\tag{F.20}
$$

$$
HG = \sin(\theta_l) C_R G,
\tag{F.21}
$$

which gives us

$$
BH = \cos(\theta_l)\frac{L_B}{2} - \sin(\theta_l)\frac{l_B}{2}.
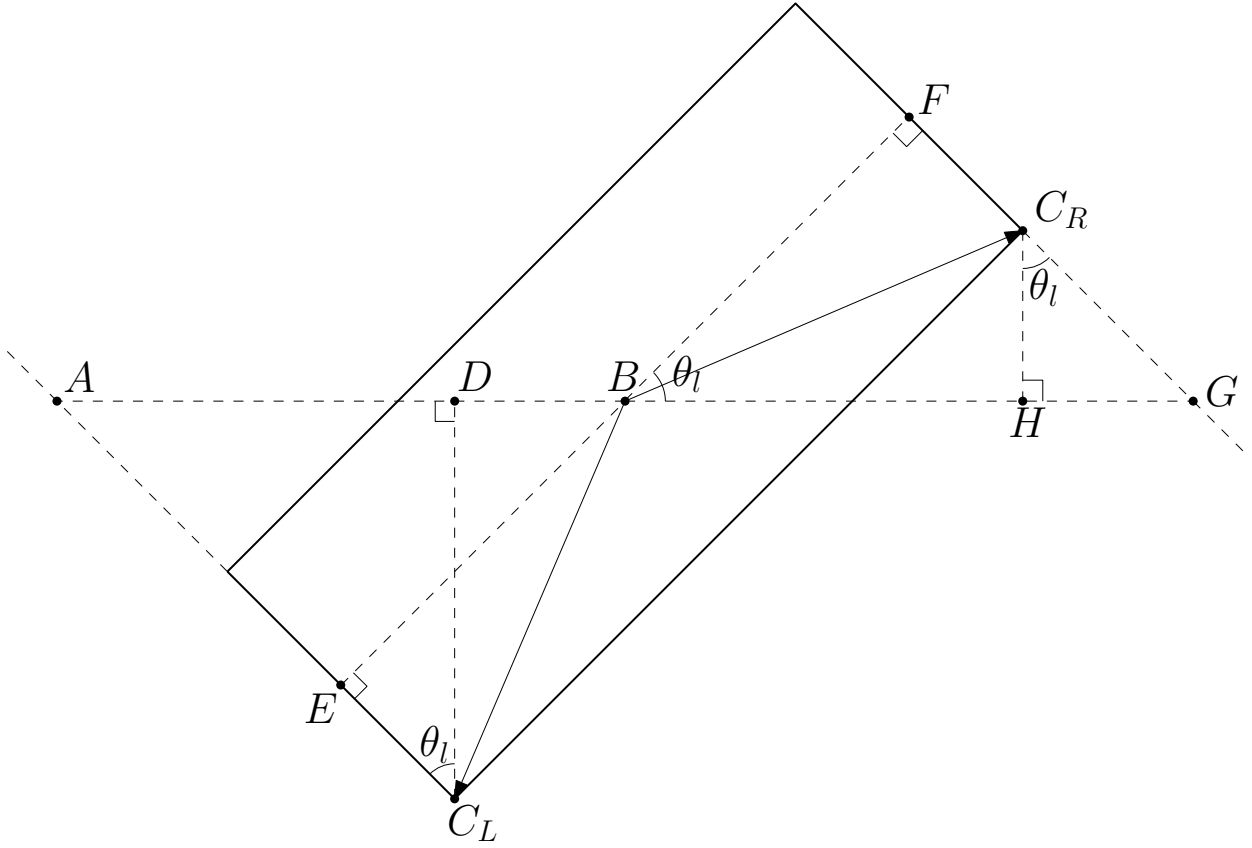\tag{F.22}
$$

Figure F.2: *Geometry of the box, used to determine the position vectors of contactpoints C_L and C_R.*

With HC_R and BH known, the position vector of C_R is

$$r_{C_R} = \begin{bmatrix} x_l + \cos(\theta_l)\frac{L_B}{2} - \sin(\theta_l)\frac{l_B}{2} \\ y_l + \sin(\theta_l)\frac{L_B}{2} - \cos(\theta_l)\frac{l_B}{2} \\ 0 \end{bmatrix}^T \vec{e}^1. \tag{F.23}$$

Using a similar approach for C_L we find

$$r_{C_L} = \begin{bmatrix} x_l + \cos(\theta_l)\frac{L_B}{2} + \sin(\theta_l)\frac{l_B}{2} \\ y_l - \sin(\theta_l)\frac{L_B}{2} - \cos(\theta_l)\frac{l_B}{2} \\ 0 \end{bmatrix}^T \vec{e}^1. \tag{F.24}$$

The guard functions g_{N1} and g_{N2} are defined as

$$g_{N1} = \vec{r}^1_{C_L} \vec{e}^1_2 - l_p = y_l - \frac{l_P}{2} - \sin(\theta_l)\frac{L_B}{2} - \cos(\theta_l)\frac{l_B}{2} = 0, \tag{F.25}$$

$$g_{N2} = \vec{r}^1_{C_R} \vec{e}^1_2 - l_p = y_l - \frac{l_P}{2} + \sin(\theta_l)\frac{L_B}{2} - \cos(\theta_l)\frac{l_B}{2} = 0, \tag{F.26}$$

Since we are in a 2D-environment, the tangential reaction forces have the same dimensions as the normal reaction-forces. Therefore Equations (**??**), (**??**) and (**??**) can now be considered as, respectively,

$$\boldsymbol{g}_T = \begin{bmatrix} g_{Ti_1}; g_{Ti_2}; ...; g_{Ti_c} \end{bmatrix} \in \mathbb{R}^c \tag{F.27}$$

$$\boldsymbol{\Lambda}_T = \begin{bmatrix} \Lambda_{Ti_1}; \Lambda_{Ti_2}; ...; \Lambda_{Ti_c} \end{bmatrix} \in \mathbb{R}^c \tag{F.28}$$

$$\boldsymbol{W}_T = \begin{bmatrix} \boldsymbol{w}_{Ti_1}; \boldsymbol{w}_{Ti_2}; ...; \boldsymbol{w}_{Ti_c} \end{bmatrix}. \in \mathbb{R}^{n \times c} \tag{F.29}$$

The velocity vectors $\dot{r}_{C_L}$ and $\dot{r}_{C_R}$ are found by taking the time-derivative of r_{C_L} and r_{C_R}, and can be written as

$$\dot{r}_{C_L} = \begin{bmatrix} \dot{x}_l - \dot{\theta}_l \sin(\theta_l)\frac{L_B}{2} + \dot{\theta}_l \cos(\theta_l)\frac{l_B}{2} \\ \dot{y}_l - \dot{\theta}_l \cos(\theta_l)\frac{L_B}{2} + \dot{\theta}_l \sin(\theta_l)\frac{l_B}{2} \\ 0 \end{bmatrix} =: \begin{bmatrix} \dot{g}_{T1} \\ \dot{g}_{N1} \\ 0 \end{bmatrix}, \tag{F.30}$$

$$\dot{r}_{C_R} = \begin{bmatrix} \dot{x}_l - \dot{\theta}_l \sin(\theta_l)\frac{L_B}{2} - \dot{\theta}_l \cos(\theta_l)\frac{l_B}{2} \\ \dot{y}_l + \dot{\theta}_l \cos(\theta_l)\frac{L_B}{2} + \dot{\theta}_l \sin(\theta_l)\frac{l_B}{2} \\ 0 \end{bmatrix} =: \begin{bmatrix} \dot{g}_{T2} \\ \dot{g}_{N2} \\ 0 \end{bmatrix}, \tag{F.31}$$

with $\dot{g}_{Ni}$ and $\dot{g}_{Ti}$ the normal and tangential relative velocities. From (**??**) and (**??**) we can write

$$\dot{\boldsymbol{g}}_N = \boldsymbol{W}_N^T \boldsymbol{v} = \begin{bmatrix} \dot{y}_l - \dot{\theta}_l \cos(\theta_l)\frac{L_B}{2} + \dot{\theta}_l \sin(\theta_l)\frac{l_B}{2} \\ \dot{y}_l + \dot{\theta}_l \cos(\theta_l)\frac{L_B}{2} + \dot{\theta}_l \sin(\theta_l)\frac{l_B}{2} \end{bmatrix}, \tag{F.32}$$

$$\dot{\boldsymbol{g}}_T = \boldsymbol{W}_T^T \boldsymbol{v} = \begin{bmatrix} \dot{x}_l - \dot{\theta}_l \sin(\theta_l)\frac{L_B}{2} + \dot{\theta}_l \cos(\theta_l)\frac{l_B}{2} \\ \dot{x}_l - \dot{\theta}_l \sin(\theta_l)\frac{L_B}{2} - \dot{\theta}_l \cos(\theta_l)\frac{l_B}{2} \end{bmatrix}, \tag{F.33}$$

from which we can deduce

$$\boldsymbol{W}_N^T = \begin{bmatrix} 0 & 1 & -\cos(\theta_l)\frac{L_B}{2} + \sin(\theta_l)\frac{l_B}{2} & 0 \\ 0 & 1 & \cos(\theta_l)\frac{L_B}{2} + \sin(\theta_l)\frac{l_B}{2} & 0 \end{bmatrix}, \tag{F.34}$$

$$\boldsymbol{W}_T^T = \begin{bmatrix} 0 & 1 & -\sin(\theta_l)\frac{L_B}{2} + \cos(\theta_l)\frac{l_B}{2} & 0 \\ 0 & 1 & -\sin(\theta_l)\frac{L_B}{2} - \cos(\theta_l)\frac{l_B}{2} & 0 \end{bmatrix}. \tag{F.35}$$

Now we have all the information to write down the local constrained dynamics

$$\boldsymbol{M}_l(\boldsymbol{q}_l)\dot{\boldsymbol{v}}_l - \boldsymbol{H}_l(\boldsymbol{q}_l, \boldsymbol{v}_l) = \boldsymbol{S}_l(\boldsymbol{q}_l)\boldsymbol{u} + \boldsymbol{W}(\boldsymbol{q}_l)\boldsymbol{\Lambda}, \tag{F.36}$$

with

$$\boldsymbol{W}(\boldsymbol{q}_l) := \begin{bmatrix} \boldsymbol{W}_N & \boldsymbol{W}_T \end{bmatrix} \text{ and } \boldsymbol{\Lambda} := \begin{bmatrix} \boldsymbol{\Lambda}_N \\ \boldsymbol{\Lambda}_T \end{bmatrix}. \tag{F.37}$$

Appendix G

Simulation Design

G.1   Reference Trajectory Design